1993-12

Neural Representations for Sensory-Motor Control, III: Learning a Body-Centered Representation of 3-D Target Position

NEURAL REPRESENTATIONS FOR SENSORY-MOTOR CONTROL, III: LEARNING A BODY-CENTERED REPRESENTATION OF 3-D TARGET POSITION

Frank H. Guenther, Daniel Bullock, Douglas Greve, and Stephen Grossberg

June 1993

Revised: December 1993

Technical Report CAS/CNS–93–045

Boston University Center for Adaptive Systems and
Department of Cognitive and Neural Systems
111 Cummington Street
Boston, MA 02215

NEURAL REPRESENTATIONS FOR SENSORY-MOTOR CONTROL, III: LEARNING A BODY-CENTERED REPRESENTATION OF 3-D TARGET POSITION

by

Frank H. Guenther†, Daniel Bullock‡, Douglas Greve§, and Stephen Grossberg*
Center for Adaptive Systems
and
Department of Cognitive and Neural Systems
Boston University
111 Cummington Street
Boston, MA 02215

Journal of Cognitive Neuroscience, in press

June, 1993
Revised: December, 1993

Technical Report CAS/CNS-TR-93-045
Boston, MA: Boston University

Requests for reprints should be sent to:
Stephen Grossberg
Center for Adaptive Systems
Boston University
111 Cummington Street
Boston, MA 02215

---

† Supported in part by the Air Force Office of Scientific Research (AFOSR F-49620-92-J-0499) and the National Science Foundation (NSF IRI-87-16960 and NSF IRI-90-24877).

‡ Supported in part by the National Science Foundation (NSF IRI-87-16960 and NSF IRI-90-24877) and the Office of Naval Research (ONR N00014-92-J-1309).

§ Supported in part by the National Science Foundation (NSF IRI-87-16960 and NSF IRI-90-24877).

* Supported in part by the Air Force Office of Scientific Research (AFOSR F49620-92-J-0499), the National Science Foundation (NSF IRI-87-16960 and NSF IRI-90-24877), and the Office of Naval Research (ONR N00014-92-J-1309).

Acknowledgements: The authors wish to thank Cynthia E. Bradford and Diana J. Meyers for their valuable assistance in the preparation of the manuscript.

ABSTRACT

A neural model is described of how the brain may autonomously learn a body-centered representation of 3-D target position by combining information about retinal target position, eye position, and head position in real time. Such a body-centered spatial representation enables accurate movement commands to the limbs to be generated despite changes in the spatial relationships between the eyes, head, body, and limbs through time. The model learns a vector representation—otherwise known as a parcellated distributed representation—of target vergence with respect to the two eyes, and of the horizontal and vertical spherical angles of the target with respect to a cyclopean egocenter. Such a vergence-spherical representation has been reported in the caudal midbrain and medulla of the frog, as well as in psychophysical movement studies in humans. A head-centered vergence-spherical representation of foveated target position can be generated by two stages of opponent processing that combine corollary discharges of outflow movement signals to the two eyes. Sums and differences of opponent signals define angular and vergence coordinates, respectively. The head-centered representation interacts with a binocular visual representation of non-foveated target position to learn a visuomotor representation of both foveated and non-foveated target position that is capable of commanding yoked eye movements. This head-centered vector representation also interacts with representations of neck movement commands to learn a body-centered estimate of target position that is capable of commanding coordinated arm movements. Learning occurs during head movements made while gaze remains fixed on a foveated target. An initial estimate is stored and a VOR-mediated gating signal prevents the stored estimate from being reset during a gaze-maintaining head movement. As the head moves, new estimates are compared with the stored estimate to compute difference vectors which act as error signals that drive the learning process, as well as control the on-line merging of multimodal information.

1. Spatial Representations for the Neural Control of Flexible Movements

This article describes neural network models of how the brain learns spatial representations with which to control sensory-guided and memory-guided eye and limb movements. These spatial representations are expressed in both head-centered coordinates and body-centered coordinates because the eyes move within the head, whereas the head, arms, and legs move with respect to the body. A model for learning an invariant body-centered representation of 3-D target position is developed. Models for learning an invariant head-centered representation of 3-D target position are described elsewhere (Grossberg, Guenther, Bullock, and Greve, 1993).

One general design theme that underlies many of our results explores the need for spatial representations—as distinct from perceptual, cognitive, or motor representations—in the control of goal-oriented behaviors. In this regard, it is well-known that visual inputs activate a "what" processing stream as well as a "where" processing stream within the brain (Goodale and Milner, 1992; Mishkin, Ungerleider, and Macko, 1983; Ungerleider and Mishkin, 1982). The "what" processing stream leads to visual recognition of external objects. It includes brain regions such as visual cortex and inferotemporal cortex. The "where" processing stream leads to spatial localization of objects, spatial attention shifts, and action. It includes brain regions such as visual cortex, superior colliculus, parietal cortex, and premotor cortex. "Where" processing is illustrated by the following competence.

Imagine that your right hand is moved by an external force to a new position in the dark, so that neither visual cues nor self-controlled outflow movement commands are available to encode the right hand's new position. Despite the absence of vision and self-controlled volition, it is easy to move your left hand to touch your right hand in its new location. The motor coordinates that represent the position of your right hand are different from the motor coordinates that your left arm realizes in order to touch it. Some representation needs to exist that mediates between the different motor coordinates of the two arms. This mediating scheme is the spatial representation. This example illustrates that different motor plans, whether for the control of one arm or two, are often used to reach a prescribed position in space. The problem of how animals can reach a fixed target in multiple ways is often called the "problem of motor equivalence" (e.g., Bernstein, 1967; Hebb, 1949). A properly defined spatial representation is a prerequisite to discovering a biologically relevant solution of the motor equivalence problem. The model introduced herein forms part of a proposed solution to the motor equivalence problem (Bullock, Grossberg, and Guenther, 1993).

The spatial representations described below have been led are built up from the same types of computations that are used to control motor commands. This observation leads

to a second general design theme of our work: we inquire into the natural form of neural computations that are appropriate for representation and control of a bilaterally symmetric body. These include opponent interactions between pairs of antagonistic neurons that measure one or another type of spatial or motor offset with respect to an axis of symmetry. An opponent model was developed in Greve, Grossberg, Guenther, and Bullock (1993) that computes a head-centered spatial representation of 3-D targets that are foveated by both eyes. This representation arises naturally from the geometry of the oculomotor system and relates closely to the geometry of the vestibular system (e.g., Blanks, Curthoys, Bennett and Markham, 1985; Ezure and Graf, 1984; Graf, 1988). Grossberg, Guenther, Bullock, and Greve (1993) further showed how to combine binocular visual information with the foveated target representation to generate an invariant head-centered spatial representation for both foveated and non-foveated 3-D target positions. A head-centered spatial representation of non-foveated targets is needed to look at new targets with the eyes and to reach towards these targets with the limbs.

The current article describes how this head-centered spatial representation can be combined with motor information concerning neck muscle lengths to form a body-centered spatial representation that is invariant under head or eye movements. A body-centered representation of space is useful for performing goal-oriented reaches with the arms, since the controlled variables for reaches (e.g., muscle lengths or joint angles) determine the position of the hand with respect to the body. Learning of this body-centered representation takes advantage of the geometry of head movements, which are limited by the biomechanics of the neck to preferred axes that are closely related to the head-centered representation described above (Vidal, de Waele, Graf, and Berthoz, 1988; Vidal, Graf, and Berthoz, 1986). The neural organization of head movement control along such preferred axes has been described by Masino and Knudsen (1990).

Learning of both the head-centered and body-centered representations takes place in variants of a Vector Associative Map, or VAM, circuit (Gaudiano and Grossberg, 1991). Learning in a VAM occurs via the use of difference vectors, which compute the error signals that drive the learning process. The same difference vectors also control the on-line merging of multimodal information into the final map representation. These dual roles of difference vectors characterize VAM dynamics. VAM properties have elsewhere proven useful for learning spatial-to-motor mappings (Gaudiano and Grossberg, 1991; Grossberg and Kuperstein, 1989, Chapter 4) and for explaining data about human trajectory formation (Bullock and Grossberg, 1988; Bullock, Grossberg, and Guenther, 1993; Gaudiano and Grossberg, 1991). The representation of differences or directions by sensory-motor areas of the nervous system

is well documented (e.g., Alexander and Crutcher, 1990a, 1990b; Caminiti, Johnson, and Urbano, 1990; Crutcher and Alexander, 1990; Georgopoulos *et al.*, 1982; 1984; Kalaska and Crammond, 1992; Mays and Sparks, 1980).

The next section surveys key geometrical and psychophysical considerations pertinent to the model. Section 3 summarizes how two successive stages of opponent interactions can generate the type of head-centered representation that is suggested by psychophysical and neurobiological data. Sections 4–8 describe neural networks for transforming this head-centered representation into an invariant body-centered representation of target position. These networks rely only on information arising within the action-perception cycle to resolve ambiguities—caused by mobile eyes and head—regarding the locations of objects relative to the body.

2. Geometry of Object Localization

During eye-hand coordination, both eyes typically fixate a target before or while a hand reaches towards it. Vision, in particular the binocular disparity of an object's image on the retinas of both eyes, provides important cues to the relative 3-D position of an object with respect to the head. Such visual information is, however, often insufficient for accurate reaching towards a binocularly fixed target. Binocular disparity, by itself, does not provide unambiguous information about target direction or absolute distance. For example, if each eye fixates a different location in the interior of a homogeneous object, then the two monocular images of the object's interior can be binocularly fused, but the binocular disparities of the object's boundaries will change with every change in the fixation points of the two eyes. These binocular disparity changes occur without a change in the object's distance from the observer. Thus binocular disparity is not a reliable cue to absolute distance in any situation of this type.

Another limitation of binocular disparity cues can arise even if both eyes fixate the same location in space. Then the binocular disparity of this location on the retinas equals zero, no matter how near or far the object may be from the observer. Thus, small fixated objects cannot accurately be reached using only information about binocular disparity. Since our primary goal in the present article is to analyse how reaching towards fixated objects is controlled, we need to consider other sources of information than retinal, or visual, information.

The bilaterally symmetric organization of the body provides another, non-visual source of information for computing absolute distance of a fixated target from an observer's head and body. When the eyes binocularly fixate a target, the angle between the lines of gaze at the point of intersection can be used to compute the absolute distance and direction

of the fixation point with respect to the head. Such extraretinal information may also be used to complement visual processing to derive better estimates of the absolute distance and direction of visually detected but non-fixated objects.

Figure 1

Figure 1 shows how the intersection point of the lines of sight of the two eyes converges toward the nose as the two eyes rotate to foveate increasingly close objects that are straight ahead. The rotation centers of the two eyes together with the fixated point on the object form a triangle. The angles of the two eyes in their orbits thus jointly specify the angle γ between the lines of sight that intersect at the fixation point. This angle is called the *binocular parallax* (Foley, 1980). The triangular structure also allows an internal measure of net ocular *vergence*—the extent to which the eyes are rotated towards the nose—to serve as one basis for estimating the distance from egocenter to a binocularly foveated object. The angle γ will henceforth be used as a measure of vergence. The head-centered representation of space derived here approximates vergence as a distance measure, with coordinates specifying horizontal and vertical target direction completing the 3-D representation.

Figure 2

Figure 2a shows the relationship between vergence and the radial distance of a target from the head. This figure illustrates that the dynamic range of a representation based on vergence is heavily weighted towards targets near the observer. Targets within reach of the observer can be represented with the high accuracy necessary for succesful reaching, but the accuracy of representation for targets further out of reach decreases due to smaller changes in vergence per unit change of distance. This property allows a physical system with limited dynamic range to efficiently represent space, since positions of important targets (i.e., those near the observer) are represented with high accuracy, and positions of targets that are far away can still be roughly approximated. Figure 2b reprints data from Sakata, Shibutani, and Kawano (1980) on a class of visual fixation neurons that they discovered in area 7a of posterior parietal cortex. These neurons were described as depth-selective and this plot shows that their discharge rate fell off with target distance in a manner strikingly similar to the vergence-distance function of Figure 2a.

A similar property can be seen in the retinotopic coding of visual space by visual cortex (e.g., Rojer and Schwartz, 1990). Figure 2c (adapted from Kandel, 1985) shows the function relating visual acuity to distance from the fovea. This curve shows a use of dynamic range very similar to that of Figure 2a, suggesting that the nervous system may use different neural circuitry to achieve similar efficiency of coding for body-centered and retinotopic

representations of visual space.

The two other coordinates in the head-centered representation of 3-D space are also derived from estimates of the position of both eyes in their orbits. Figure 3 describes the geometry of 3-D target localization in terms of a spherical coordinate frame. The origin of this coordinate system, called the cranial egocenter, lies at the midpoint between the two eyes. Thus the representation is "cyclopean". The head-centered horizontal angle or azimuth, θ_H, and the vertical angle or elevation, ϕ_H, measure deviations from straight-ahead gaze. The radial distance R_H in the spherical coordinate frame of Figure 3 is replaced by vergence γ in the representation of 3-D space described below. Figure 4 relates the geometry of the cyclopean horizontal angle θ_H to the angles θ_L and θ_R subtended by the left eye and right eye, respectively.

Figure 3

Figure 4

Experimental support for such a 3-D coordinate system can be found in data on the role of extraretinal information in visual object localization (e.g., Blank, 1978; Foley, 1980; Sakata *et al.*, 1980) and on parcellated population codes of 3-D target location (Grobstein, 1991; Hollerbach, Moore, and Atkeson, 1986; Soechting and Flanders, 1989). These and related data will be discussed below. First, a head-centered 3-D coordinate system consistent with the evidence is described in the next section, in order to suggest how such a representation can naturally arise from simple neural computations.

3. Opponent Sums and Differences Represent Foveated 3-D Target Positions

A head-centered representation of a foveated target can be formed by binocularly combining outflow movement signals from the tonically active cells that control the position of each eye. This can be done in two stages of opponent processing, as shown in Figure 5. First, opponent interactions combine the outputs of the cells that control the agonist and antagonist muscles of each eye. These opponent interactions give rise to opponent pairs of cells the sum of whose activity is approximately constant, or normalized. Next, the normalized outputs from both eyes are combined in two different ways to generate a head-centered spatial representation of the binocular fixation point. In particular, opponent cells from each eye generate inputs of opposite sign (excitatory and inhibitory) to their target cells at the next processing stage. As illustrated in Figure 5, one combination gives rise to a cell population whose activity h_2 approximates the angular spherical coordinate θ_H. The other combination gives rise to a cell population whose activity h_5 approximates the binocular vergence γ, which in turn is a measure of the radial distance R_H. The two combinations

generate head-centered coordinates by computing a sum and a difference of the normalized opponent inputs from both eyes. Such a general strategy for combining signals is well-known in other neural systems, such as color vision. For example, a sum $L + M$ of signals from two color vision channels estimates luminance, whereas a difference $L - M$ estimates color (DeValois and DeValois, 1975; Mollon and Sharpe, 1983). Thus the computations that may be used to control reaching in 3-D space seem to derive from a broadly used principle of neural computation.

Figure 5

The neural mechanism for normalizing the total activity of opponent cells uses a shunting on-center off-surround network (Grossberg, 1982); that is, an opponent interaction wherein the target cells obey a membrane equation (Hodgkin, 1964; Katz, 1966). In particular, suppose that the agonist and antagonist cells that control the horizontal position of the left eye have activities L_1 and L_2, respectively. Let the normalized opponent cells in the shunting network have activities l_1 and l_2. Suppose that

$$\frac{d}{dt}l_1 = -Al_1 + (1 - l_1)L_1 - l_1L_2 \tag{1}$$

and

$$\frac{d}{dt}l_2 = -Al_2 + (1 - l_2)L_2 - l_2L_1. \tag{2}$$

By equation (1), activity L_1 excites l_1 whereas activity L_2 inhibits l_1. The opposite is true in equation (2). Parameter A is the decay rate. At equilibrium, $\frac{d}{dt}l_1 = \frac{d}{dt}l_2 = 0$, so (1) and (2) imply that

$$l_1 = \frac{L_1}{A + L_1 + L_2} \tag{3}$$

and

$$l_2 = \frac{L_2}{A + L_1 + L_2}. \tag{4}$$

Adding (3) and (4) shows that

$$l_1 + l_2 = \frac{L_1 + L_2}{A + L_1 + L_2}. \tag{5}$$

Thus if $A \ll L_1 + L_2$,

$$l_1 + l_2 \cong 1. \tag{6}$$

Since L_1 and L_2 are opponent signals, one goes up when the other goes down, so their sum $L_1 + L_2$ can easily be kept larger than parameter A. Small deviations from complete normalization do not affect the results.

The approximation (6) will be used below for all normalized pairs of opponent cells. In particular, we assume that the activities of opponent cell populations that control agonist-antagonist muscle pairs are normalized so that the total activity of each cellular pair is fixed at unity. This ensures that increasing the activity of the agonist control cell results in a corresponding decrease in the activity of its antagonist control cell. Figure 5 shows the two cellular pairs needed to control θ_L and θ_R. These pairs are labeled by the variables l_1, l_2 and r_1, r_2, which measure corresponding cellular activities. Thus, the following equations define the internal representations of the horizontal angle of each eye:

$$l_1 + l_2 = 1 \quad \text{and} \quad r_1 + r_2 = 1, \tag{7}$$

$$\theta_L = -90° + 180° \times l_2 \quad \text{and} \quad \theta_R = -90° + 180° \times r_2 \tag{8}$$

where l_i indicates the activity of left eye cell population i and r_i indicates the activity of right eye cell population i.

Internal representations for the vertical angles of left and right eyes may be defined similarly. Thus

$$l_3 + l_4 = 1 \quad \text{and} \quad r_3 + r_4 = 1, \tag{9}$$

$$\phi_L = -90° + 180° \times l_4 \quad \text{and} \quad \phi_R = -90° + 180° \times r_4. \tag{10}$$

To provide a head-centered representation of foveated 3-D target positions, the outflow signals l_1, l_2, l_3, and l_4 are binocularly combined. Let the cell populations $h_i, i = 1, 2, \ldots 6$, form the basis for this head-centered spatial representation. These populations are also arranged in antagonistic pairs. First we define cell activities h_1, h_2, h_3, and h_4 that linearly approximate the following estimates of θ_H and ϕ_H:

$$h_1 + h_2 = 1 \quad \text{and} \quad h_3 + h_4 = 1, \tag{11}$$

$$\theta_H = -90° + 180° \times h_2 \quad \text{and} \quad \phi_H = -90° + 180° \times h_4. \tag{12}$$

These head-centered binocular representations of θ_H and ϕ_H emerge if a shunting on-center off-surround network simply averages the corresponding monocular components derived from corollary discharges of left and right eye muscle commands. Figure 5 shows the connectivity of this network for the cell activity h_2 which represents θ_H. In particular,

$$\frac{d}{dt}h_2 = -Bh_2 + (1 - h_2)(l_2 + r_2) - h_2(l_1 + r_1), \tag{13}$$

where B is the decay rate. Solving this equation at equilibrium ($dh_2/dt = 0$) yields

$$h_2 = \frac{l_2 + r_2}{B + l_1 + r_1 + l_2 + r_2}. \tag{14}$$

Since $l_1 + l_2 \cong 1$ and $r_1 + r_2 \cong 1$, choosing a small decay parameter B leads to the approximations:

$$h_1 \cong \frac{l_1 + r_1}{2} \quad \text{and} \quad h_2 \cong \frac{l_2 + r_2}{2}, \tag{15}$$

so that (11) holds.

To evaluate the adequacy of this internal representation of θ_H, a distortion measure was calculated in Greve *et al.* (1993) by dividing the change in the internally represented angle of two successively foveated points by the actual change in angle of the successively foveated points for small changes throughout the workspace. The distortion measure was calculated for a workspace defined by $-45° < \theta_H < 45°$, $-45° < \phi_H < 45°$, and 3 inches $< R_H < 30$ inches (7.6 cm $< R_H <$ 76 cm). This workspace was chosen to approximate the cone within which both binocular foveation and reaching to a target are possible in humans. The distortion in this range is less than 15%, with essentially 0% distortion for $R_H > 5$ inches. Thus, the opponent network defined above provides an accurate mechanism for computing an internal representation of θ_H. Likewise, the distortion measure for ϕ_H showed that the normalized binocular opponent network provides an accurate internal representation of ϕ_H in all but the most extreme portions of the workspace.

To see how opponent computation leads to a representation of distance from the head, note that vergence, which is systematically related to distance from the head, is proportional to the difference between r_1 (the outflow command to the medial rectus of the right eye) and l_1 (the outflow command to the lateral rectus of the left eye). As in Figure 5, define antagonistic cell populations with activities h_5 and h_6 for internal representation of vergence. The cell population with activity h_5 receives excitatory inputs l_2 and r_1 from cells controlling the medial recti of both eyes and inhibitory inputs l_1 and r_2 from cells controlling the lateral recti of both eyes. Then activity h_5 obeys the equation

$$\frac{d}{dt}h_5 = -Ch_5 + (1 - h_5)(r_1 + l_2) - (h_5 + D)(l_1 + r_2). \tag{16}$$

At equilibrium,

$$h_5 = \frac{r_1 + l_2 - Dl_1 - Dr_2}{C + r_1 + r_2 + l_1 + l_2}. \tag{17}$$

Because $r_1 + r_2 = 1$ and $l_1 + l_2 = 1$, equation (17) can be rewritten as

$$h_5 = \frac{1 - D}{C + 2} + \frac{1 + D}{C + 2}(r_1 - l_1). \tag{18}$$

If $D = 1$ and $C = 0$, then

$$h_5 = r_1 - l_1. \tag{19}$$

In this case, subjective vergence equaled physical vergence. If, however, $C > 0$ and $D < 1$, corresponding to the biologically realistic assumptions of non-zero decay and a hyperpolarization magnitude less than the depolarization magnitude, then the slope $(1 + D)(C + 2)^{-1}$ of h_5 versus $r_1 - l_1$ is less than one, and the intercept $(1 - D)(C + 2)^{-1}$ of the function is positive. Such values match the Foley (1980) estimate from psychophysical data of the internal representation of binocular parallax. Greve *et al.* (1993) discuss psychophysical data that are consistent with this representation.

4. Vector Representations of 3-D Target Position: Distributed Parcellated Representations in the Frog

Given the simplicity of this solution to the problem of using binocular signals to construct a 3-D vector representation of target locations, it might be supposed that such a solution would be discovered at an early point in evolution. In fact, such a 3-D vector representation of target location seems to exist in frogs. Grobstein (1991) reported data indicating egocentric coding of distance, horizontal angle, and vertical angle in distinct cell populations, each of whose activation levels codes the target's coordinate value on one of these three dimensions.

Grobstein (1991) summarized a number of relevant experiments, particularly those of Grobstein and Staradub (1989) and of Masino and Grobstein (1989), that reported data concerning a head-centered or body-centered coordinate representation in the frog's caudal midbrain and medulla. This representation differs from more peripheral retinal and tectal representations. The cell properties of the representation are strikingly similar to those of the spherical vergence representation that was described above. In particular, Grobstein (1991, p. 130) noted that the angular head-centered variables are radial, not Cartesian, as is also true of the angular variables θ_H and ϕ_H. Moreover, "increasing levels of activity in the distance pathways code for stimulus locations nearer to the frog" (p. 132), as is also true of a vergence-like measure of distance. Grobstein (1991) also asserted that this representation is a parcellated, distributed representation. By this he means a *vector* representation, such as $(\theta_H, \phi_H, \gamma)$, whose individual components code a variable by its activity level, as opposed to a *map* representation that codes each variable by a distinct position in a spatially organized array. Thus Grobstein (1991, p. 132) noted that "the value of components of the parcellated representation are coded in terms of the level of activity across a population of neurons, rather than in terms of which particular elements of a population of neurons are active". After reviewing a number of other organisms where this type of representation seems to exist, he concluded that "in general terms, it may make sense to think of sensorimotor transforms in terms of a transformation from place coding to population activity coding, rather than as a transformation from place coding to frequency coding" (p. 135).

Such a parcellated, or vector, representation should occur at processing stages subsequent to spatial mapping stages at which visual, motor, and visuomotor information are first represented and combined. For example, in Grossberg *et al.* (1993), it was shown how visual and motor information could be combined to autonomously learn a head-centered vector representation of both foveated and nonfoveated target position. Such a representation can be used to command yoked eye movements to foveate the target. This article shows how a body-centered vector representation can be learned, again based upon information that is organized in spatial maps.

5. Learning a Body-Centered Representation of 3-D Space

The remainder of this article addresses the formation of a body-centered representation of 3-D target positions using the head-centered representation described in the previous sections coupled with information concerning the position of the head with respect to the torso. The network uses signals generated automatically during changes of visual fixation. In a typical episode:

1. The representation of a novel, initially non-foveal visual target wins an internal competition that determines the next target to be foveated, and a saccade is made to this target.
2. Information about position computed in head coordinates is combined with information about neck muscle states to yield an estimate of target location relative to the body that is stored during a subsequent head movement.
3. Next, neck muscles rotate the head (either randomly or to point the nose towards the target) while the eyes make a counter rotation, mediated by the vestibulo-ocular reflex (VOR), to ensure continued foveation during the head movement.
4. During the head movement and ocular counter-rotation, both internal representations of the target's location in head coordinates and internal representations of neck muscle lengths change while the stored representation of target position in body coordinates remains constant.

If head-centered and neck muscle length information interact correctly to estimate target location in body coordinates, then this estimate will remain invariant during head rotation and ocular counter-rotation. If the mapping is not well-tuned, then a mismatch will develop during the head rotation between the network's current estimate and the estimate stored prior to the head rotation. This mismatch serves as an error signal to a learning process that improves the network's mapping of neck muscle length and head coordinate signals into target position relative to the body. The stage that registers the mismatch is called a *difference*

vector (DV) stage, because errors are registered on a component-by-component basis. This DV error detection and learning process forms part of the direct flow of information that combines retinal, eye position, and neck position signals into a body-centered representation. DV-based learning is a variant of the Vector Associative Map (VAM) of Gaudiano and Grossberg (1991). VAM learning is capable of operating in real time, requires no external teacher, and combines mechanisms known to be separately available *in vivo*.

A mechanism is needed to prevent the target estimate that is stored before the head movement from being corrupted by the changing estimates that are caused by the head movement. In the model, a gate is open between head movements and allows an estimate of target position to be stored. A head movement that maintains gaze on the foveated target closes the gate to prevent the stored estimate from changing while the head moves. We assume that VOR-related circuitry opens and closes this gate as it causes counterrotation by the eyes to maintain gaze on the target (Bizzi, Kalil, and Tagliasco, 1971; Dichgans, Bizzi, Morasso, and Tagliasco, 1973; Morasso, Bizzi, and Dichgans, 1973; Tomlinson and Bahra, 1986). The gate allows a DV to estimate the error caused by the head movement, and to use this error, in the VAM learning circuit described below, to autonomously learn a body-centered vector representation of target position.

The body-centered representation that is learned approximates a spherical coordinate frame that is similar to the spherical coordinate frame approximated by the head-centered representation. The relationship between the head-centered and body-centered spherical coordinate frames is shown in Figure 6. The origin of the body-centered system is the same as the origin of the head-centered system when the head is pointed straight ahead. The body-centered frame also uses the same three spherical coordinates as the head-centered system, denoted by (θ_B, ϕ_B, R_B). When the head is pointed straight ahead, the head-centered representation (θ_H, ϕ_H, R_H) is identical to the body-centered representation (θ_B, ϕ_B, R_B). When the head is moved from straight ahead, however, the head-centered frame moves with the head while the body-centered frame remains stationary. Denote by θ_N (N for neck angle) the horizontal angle and by ϕ_N the vertical angle of the head with respect to the torso (see Figure 6).

Figure 6

The following simplifying approximations are made in the simulations:

1. The radius R_B of the body-centered frame is assumed to be approximately equal to the radius R_H of the head-centered frame;
2. The horizontal and vertical angles (θ_B, ϕ_B) of the body-centered frame are approximated

by the equations $\theta_B = \theta_H + \theta_N$ and $\phi_B = \phi_H + \phi_N$.

Due to the relatively small displacement of the head-centered origin with respect to the body-centered origin when the head is displaced from straight ahead, these approximations result in small error for all points except those very close to the eyes. Section 7 describes a neural network that learns corrections to the head-centered representation of distance from the head to allow veridical representation of this distance in a body-centered frame. This network uses a slower nonlinear learning process that supplements the fast linear learning process described in this section to correct for residual error resulting from any nonlinearities in the functions $\theta_B = f(\theta_H, \theta_N)$ and $\phi_B = f(\phi_H, \phi_N)$.

These coordinate frames are consistent with the organization of head-neck systems in humans and other vertebrates. Neck vertebrae biomechanics favor rotations of the head around preferred axes (Vidal, de Waele, Graf, and Berthoz, 1988). Movements along one axis corresponds to changes in θ_N (side-to-side or horizontal movements), whereas movements along the other axis corresponds to changes in ϕ_N (vertical movements). Further evidence for preferred axes comes from Masino and Knudsen (1990), who showed that separate neural circuits are used to control horizontal and vertical head movements in the barn owl.

The body-centered representation is invariant in the sense that it compensates for movements of the eyes in the head and of the head in the body relative to a target whose location is fixed with respect to the body. Learning to discount head movements in the body-centered representation compensates for changes in head position by negating the resulting changes in the head-centered representation of a fixed target position. In other words, $(\theta_B, \phi_B) = (\theta_H, \phi_H) + (\theta_{\text{correction}}, \phi_{\text{correction}})$, where $(\theta_{\text{correction}}, \phi_{\text{correction}})$ is a learned correction based on neck muscle information. After the transformation network is adaptively calibrated, this correction is nearly linearly related, in fact nearly equal, to the head movement (θ_N, ϕ_N) defined according to the preferred axes. This linear relation between head movements and the required correction to the head-centered representation allows very fast and accurate learning of the correction. The relationship between head movements and other possible head- and body-centered coordinate frames, such as Cartesian, is much more complex, making the transformation from a head-centered representation to a body-centered representation more difficult to learn.

Although head position (θ_N, ϕ_N) can be derived from neck muscle length information, an animal cannot without learning use this neck muscle information to accurately compensate for head movements when forming a body-centered representation. This is because the relationship between any one neck muscle length and head position is dependent upon details of the neck anatomy which vary from individual to individual and can change with time (e.g.,

due to growth). Therefore, the organism must *adaptively* find parameters that allow neck muscle length information to compensate for changes in head position. The network rapidly learns these parameters without the aid of an external teacher by capitalizing on the fact that the positions of fixed objects with respect to the body do not change while the head moves and target foveation is maintained. This allows the network to autonomously generate internal teaching signals that are derived from the flow of sensory and motor signals. The details of this process are described in the following paragraphs.

Figure 7

6. Network Description

Figure 7 illustrates the model network that was simulated. Populations corresponding to representations of R_H and R_B are omitted in this section due to the relative non-dependence upon neck movements of these variables. In the remaining network, there are five main neural population types:

1. neck muscle length populations with activities n_{ji} $(1 \leq j \leq 9,\ 1 \leq i \leq 2)$.
2. head-coordinate populations with activities h_i $(1 \leq i \leq 4)$.
3. head-neck Difference Vector (DV) populations with activities x_i $(1 \leq i \leq 4)$,
4. unnormalized body-coordinate populations with activities $b_i^{(1)}$ $(1 \leq i \leq 4)$, and
5. normalized body-coordinate populations with activities $b_i^{(2)}$ $(1 \leq i \leq 4)$.

Each head-coordinate population projects with a fixed weight connection to the corresponding DV population. Each neck muscle length population projects to every DV population through an adaptive weight connection. As noted above, the model assumes that a VOR-mediated gate modulates the interactions between the DV populations and the unnormalized body-centered representation populations. It is assumed that foveation is maintained during head movements by the VOR system. Breaking of gaze from one target to another is thus referred to as breaking of VOR fixation, and gating that occurs due to these breaks of gaze is referred to as VOR-mediated gating. However, the only functional requirement for the current network is that it can detect when a new target has been foveated, without regard to the system or type of eye movements used to maintain (or recover) foveation of the target during (or after) head movements.

The first population type represents the lengths of the neck muscles. These can arise from corollary discharge copies of outflow commands to the neck muscles and/or from proprioceptive signals originating at the muscle spindles. These populations code neck muscle lengths in agonist-antagonist coordinates. The gain of each agonist-antagonist pair was

varied from pair to pair in order to demonstrate that such variability does not impair the learning process. The simulations used nine agonist-antagonist muscle pairs. Each neck muscle was assumed to produce rotation around both of the preferred axes discussed above. That is, the lengths of the j^{th} neck muscle antagonistic pair (n_{j1}, n_{j2}) are related to the angles θ_N and ϕ_N according to the following equations:

$$n_{j1} = \frac{\theta_N + 90°}{180°} H_j + \frac{\phi_N + 90°}{180°} V_j \tag{20}$$

$$n_{j2} = H_j + V_j - n_{j1} \tag{21}$$

where H_j and V_j are gain factors that code the relative influence of the j_{th} muscle pair on the horizontal and vertical head angles, respectively. For example, a large value of H_j and a small value of V_j means that the j^{th} pair of muscles has a strong influence on horizontal angle of the head but a small influence on vertical angle of the head. The value for each gain in the simulations was chosen randomly between 0.25 and 1.0. All neck muscle length populations project to all head-neck DV populations. For example, a neck muscle length population that primarily codes horizontal angle (i.e., one with very small V_j) initially projects to all head-neck DV populations, including those that code vertical angle. For proper operation, learning within the network must ensure a small influence on the head-neck DV vertical angle populations and a larger influence on the head-neck DV horizontal angle populations. This result is confirmed by the simulations.

The second population type constitutes the head-centered representation of target position, as described in Section 3. Specifically,

$$h_1 = \frac{90° - \theta_H}{180°} \quad \text{and} \quad h_2 = \frac{90° + \theta_H}{180°}, \tag{22}$$

$$h_3 = \frac{90° - \phi_H}{180°} \quad \text{and} \quad h_4 = \frac{90° + \phi_H}{180°}. \tag{23}$$

The activities of the third population type, the head-neck DV populations, represent the difference between the stored target position at the unnormalized body coordinate activities and the current body-centered position defined by the combination of head-centered and neck muscle information. Pathways from the neck muscle activities to the DV activities can be chosen either excitatory or inhibitory. As described below, different learning laws are used for the neck-to-DV weights in the two cases. An excitatory tonic input T to the DV populations is also used in the circuit with inhibitory neck-to-DV pathways to keep the $b_i^{(1)}$ and $b_i^{(2)}$ signals nonnegative throughout the learning process. The input T is a mildly constrained parameter; simulation results discussed below verify proper operation for a wide range of T values.

As with all population activities in the model, the DV activities x_i equilibrate rapidly with respect to input changes, and thus can be described using the following equilibrium equations:

DV Activity (Excitatory Pathways)

$$x_i = h_i + \sum_{\text{all j,k}} n_{jk} z_{jki} - b_i^{(1)} \tag{24}$$

DV Activity (Inhibitory Pathways)

$$x_i = h_i + T - \sum_{\text{all j,k}} n_{jk} z_{jki} - b_i^{(1)} \tag{25}$$

Variables z_{jki} in (24) and (25) represent the adaptive weights, or long term memory (LTM) traces, that are changed through learning. Variables $b_i^{(1)}$ represent the stored body-centered target position. When a new estimate of body-centered target position is instated at the head-neck system, the head-centered signals and neck muscle signals are combined at the DV and integrated at the body-centered target position populations for storage during the subsequent head movement. Because the body-centered target populations project inhibitory pathways back to the DV populations, the $b_i^{(1)}$ populations reach equilibrium when the body-centered target representation equals the target representation formed from the head-centered signals added to the neck muscle signals. Integration occurs quickly, so that equilibrium is rapidly reached while the excitatory pathways from the DV are gated open. When the VOR is active during a head movement, these pathways are gated shut (Figure 7). Thus the body-centered estimate that is stored before the movement is not disrupted by the movement. Storage of new body-centered estimates occurs whenever VOR-mediated target tracking is broken and a new target is instated.

The $b_i^{(1)}$ populations need to track all possible displacements of a target within the body-centered frame. Since the input signals to this stage are rectified, and thus of fixed sign, the network includes inhibitory projections from each DV population to the antagonist $b_i^{(1)}$ population. For example, in addition to the excitatory links $x_1 - b_1^{(1)}$ and $x_2 - b_2^{(1)}$, the network includes inhibitory links $x_1 - b_2^{(1)}$ and $x_2 - b_1^{(1)}$. This push-pull arrangement enables both decrements and increments to be integrated. These opponent inhibitory links are omitted from Figure 7 for simplicity. Such a gated opponent integrator also appears in the VITE and VAM arm movement trajectory generator models (Bullock and Grossberg, 1988; Gaudiano and Grossberg, 1991). The following equation describes $b_i^{(1)}$ stage updating:

Gated Updating of Body-Centered Activity

$$\frac{d}{dt} b_i^{(1)} = G x_i. \tag{26}$$

where gate G is open ($G = 1$) except when the VOR is active, during which times the gate is closed ($G = 0$). The cells controlling the gating signal are thus pauser cells that are inactive during a head movement. Both excitatory and inhibitory x_i values are integrated. Given that output signals from DV cells to body-centered cells are rectified, (26) can be realized by integrating signals directly from ON cells when their activities x_i are nonnegative, and from OFF cells whose activities $-x_i$ generate nonnegative signals when the ON cell activities x_i are nonpositive.

The equilibrium activities approached by the $b_i^{(1)}$ while G is positive are computed differently if excitatory or inhibitory neck signals are used:

Body-Centered Activity (Excitatory Neck-to-DV Pathways)

$$b_i^{(1)} = h_i + \sum_{\text{all j,k}} n_{jk} z_{jki} \tag{27}$$

Body-Centered Activity (Inhibitory Neck-to-DV Pathways)

$$b_i^{(1)} = h_i + T - \sum_{\text{all j,k}} n_{jk} z_{jki}. \tag{28}$$

Equation (26) implies that after G goes off, these values are stored throughout the subsequent head movement, during which the VOR assures foveal fixation of the stationary target whose coordinates the $b_i^{(1)}$ specify.

The fifth set of populations normalize the unnormalized variable $b_i^{(1)}$ via shunting agonist-antagonist interactions:

Normalized Body-Centered Activity

$$b_1^{(2)} = \frac{b_1^{(1)}}{b_1^{(1)} + b_2^{(1)}} \quad \text{and} \quad b_2^{(2)} = \frac{b_2^{(1)}}{b_1^{(1)} + b_2^{(1)}}; \tag{29}$$

$$b_3^{(2)} = \frac{b_3^{(1)}}{b_3^{(1)} + b_4^{(1)}} \quad \text{and} \quad b_4^{(2)} = \frac{b_4^{(1)}}{b_3^{(1)} + b_4^{(1)}}. \tag{30}$$

These populations compute an agonist-antagonist body-centered target position with fixed gain. If the network is properly tuned, a linear relationship holds between activities $b_i^{(2)}$ and actual target angles measured in the body-centered frame. To assess network representations of θ_B and ϕ_B, we used a linear regression analysis to find the slopes (A, C) and intercepts (B, D) of the best fitting lines relating $b_2^{(2)}$ to θ_B and $b_4^{(2)}$ to ϕ_B. This yielded equations

$$\hat{\theta}_B = A b_2^{(2)} + B, \tag{31}$$

$$\hat{\phi}_B = C b_4^{(2)} + D. \tag{32}$$

The adaptive weights z_{jki} between the neck muscle activities n_{jk} and the DV activities x_i, when excitatory pathways are used, obeys the following learning law:

Learning Law (Excitatory Pathways)

$$\frac{d}{dt} z_{jki} = -\epsilon x_i(-E z_{jki} + n_{jk}), \tag{33}$$

where ϵ is a small learning rate parameter and E is a decay rate parameter. Weight values were updated after each trial. Learning adjusts weights in (24) so that the total excitatory input just balances the inhibitory input from the $b_i^{(1)}$ stage. When the sum of these inputs is zero, $x_i = 0$, so learning self-terminates, by (33).

If inhibitory neck to DV pathways are used, the learning law is:

Learning Law (Inhibitory Pathways)

$$\frac{d}{dt} z_{jki} = \epsilon x_i(-E z_{jki} + n_{jk}) \tag{34}$$

Learning laws of this general form have been observed *in vivo* by many neurophysiologists (e.g., Levy and Desmond, 1985; Rauschecker and Singer, 1979; Singer, 1983). This learning law is often called the instar learning law, or the gated steepest descent learning law. It was introduced into the neural network literature in Grossberg (1969) and is the learning law used in the self-organizing feature map model (Grossberg, 1976a, 1982; Kohonen, 1984) and adaptive resonance theory (Carpenter and Grossberg, 1987, 1991; Grossberg, 1976b, 1982).

7. Model Simulations of Body-Centered Learning

The following steps were used to train the network:

1) Initialize all weights to 0.0.
2) Choose a random initial head position (θ_N, ϕ_N).
3) Choose a random target position (θ_T, ϕ_T).
4) Foveate new target by adjusting h_i so that $\theta_H = \theta_T - \theta_N$ and $\phi_H = \phi_T - \phi_N$. Store this target in the body coordinate populations $b_i^{(1)}$ and $b_i^{(2)}$. Storage of the target is controlled by opening the gate G in (26). The gate closes when the VOR is active.
5) Choose a new head position while remaining foveated on current target. Change n_{ij} and adjust h_i accordingly to keep $\theta_H + \theta_N = \theta_T$ and $\phi_H + \phi_N = \phi_T$. This step corresponds to moving the head while using the VOR to keep the target foveated. In the first five sets of simulations that were carried out, the new head position was chosen from a random

distribution (either triangular or uniform) centered at $\theta_N = 0$. In the sixth and seventh sets of simulations, the new position was chosen such that $\theta_H = 0$, corresponding to moving the head to center the target in head coordinates. All these variations led to correct learning of the body-centered spatial representation.

6) Adjust the adaptive weights from the neck muscle length populations to the head-neck DV populations according to the instar learning equation (33) or (34). In the first six simulations, it was assumed that all learning occurs during periods when the head position remains fixed at the end of the movement. This approximation may be justified by the assumption that learning is slow enough that significant learning does not occur during head movements, but instead requires the longer periods of target foveation that occur with the head still. In the seventh simulation, it was assumed that all learning occurs during the head movement. The point of this simulation was to show that the self-organization process is robust in that it does not require learning to occur only with the head in a fixed position.

7) Repeat steps (3)–(7) until the learning process converges.

For all seven sets of simulations, a fourth order Runge-Kutta method with $\Delta t = 0.01$ was used with total time of integration per trial of 1.0. The learning rate parameter ϵ was 1.0, and the LTM decay parameter E in (33) or (34) was 0.1. Error was measured by averaging the absolute values of the difference between estimated body-centered target angles and the actual target angles throughout the workspace (i.e., $-45° < \theta < 45°, -45° < \phi < 45°$ for target angles, neck angles, and head-centered representation angles).

The first two simulations used excitatory pathways from the neck muscle populations to the head-neck DV populations and corresponding LTM learning law (33). In the first simulation, a uniform distribution between $-45°$ and $+45°$ was used for choosing head positions during training. The results of this simulation are shown in Figures 8, 9, and 10. Figure 8 shows average error plotted as a function of trial number. This figure indicates rapid convergence, with less than 0.1° average error after 200 targets were attempted. Figure 9 shows the internal representation (left side) and actual target position (right side) during a head movement after 20 learning trials (i.e., after foveating 20 targets). As the head moves, the internal representation of the target position also moves, even though the actual target position with respect to the body remains fixed. After 200 trials, however, the network has learned to invariantly represent the body-centered target position despite large head movements, as shown in Figure 10.

Figure 8

Figure 9

Figure 10

In the second simulation, a triangular distribution centered at 0° was used for choosing the head position during training. Again, convergence to less than 0.1° average error was rapid, with less than 400 targets required. The results for this simulation and the remainder of the simulations were very similar to Figures 8, 9, and 10, and are thus not included here. These simulations indicate that random neck movement after target foveation is sufficient to rapidly build a body-centered invariant representation of external space.

The third, fourth, and fifth sets of simulations replicate these findings using inhibitory pathways from the neck muscle populations to the head-neck DV populations and the LTM learning law (34). The third and fourth sets of simulations used a tonic input parameter $T = 6.5$ with uniform and triangular head position distributions, respectively. Again, convergence was rapid, requiring less than 200 targets in the uniform case and 400 targets in the triangular case. With this tonic input value, the dynamic range (i.e., the change in activity level of the internal representation corresponding to a given change in the external angle) of the $b_i^{(2)}$ populations was approximately the same as in simulations 1 and 2. To illustrate robustness with respect to T, simulation 5 was run using $T = 10$. Convergence occurred in fewer than 200 trials for this simulation also. However, the dynamic range of the $b_i^{(2)}$ populations dropped, indicating that an ideal level of tonic input exists. Levels increasingly different from this ideal level do not strongly affect the convergence of the network but do increase susceptibility to noise and inaccuracies of the processing units.

In the sixth simulation, the probabilistic choice for head position in the first two simulations was replaced with neck movements that centered the new targets with respect to the head. This corresponds to the natural tendency to turn the head toward a newly attended target. Training in this manner converges in less than 250 trials.

The seventh simulation set was designed to show that it is not necessary to have learning occurring only at the end of a head movement. The network was modified to allow learning only during head movements, with no learning occurring after movements have stopped. The gate G must still be used in this case to insure that the stored body-centered representation $b_i^{(1)}$ does not change during movement. The learning process can then be visualized as allowing each neck position encountered during the movement to learn a small amount about the body-centered position stored prior to movement onset. Convergence occurred in less than 500 trials for this simulation. This result, coupled with the previous simulations with learning at the end of movements, indicates that convergence will occur without the need to shut off learning at any time, provided that learning is slow relative to the process of $b_i^{(1)}$ stage updating.

8. Learning an Invariant Body-Centered Distance

Though head movements can create large discrepancies between the head-centered and body-centered angles of a target, head movements do not cause discrepancies of more than a few inches between head-centered and body-centered distances of a target. Thus in the prior section we did not propose a direct role for corollary discharges of neck motor commands in body-centered distance computations. Nevertheless head movements are pertinent to target distance estimates because, as shown in Figure 11, egocentric distance estimates based on vergence are not invariant under changes of θ_H. Thus an object moving on an arc at a fixed distance relative to a fixed head during binocular tracking would appear to have a variable distance if vergence were the sole basis of distance estimation. Although this in itself might be problematic, at least with the head fixed, the mapping between points in space and egocentric representations is one-to-one. However, a stationary object fixated during a head movement would be represented as having changed its egocentric distance during the movement. In this case, the mapping from points in space to egocentric representations is one-to-many. This would create a difficulty for any animal that attempts to learn a mapping between egocentric representations of points in space and arm configurations adequate to reach to such points. Because the latter learned mapping would be many-to-one, it would at the least take longer to learn. This extra learning time would be doubled, for example, if points needed to be reached by two different forelimbs.

Figure 11

Psychophysical data reviewed by Blank (1978, p. 89) indicate that whereas points on an isovergence curve (Figure 11) appear to be equidistant from the observer for sufficiently distant objects, there is a departure from this tendency for nearer objects, such that perceived distance becomes more accurate than if vergence remained the sole determinant of egocentric distance estimates. Moreover, Blank reported that the observed correction factor applied for near-space objects could be computed from knowledge of θ_H. In addition to such information about apparent distance, which indicates partial compensation, it would be useful to have behavioral information. In principle, verbal reports of apparent distance may underestimate actual compensation for variations in θ_H. These might be revealed in non-verbal tasks such as blind reaching to targets seen eccentrically before closing the eyes. In fact, blind reaching studies have documented relatively accurate reaches, though accuracy for the radial distance component of blind reaches has been reported to be poorer than horizontal and vertical angles (Soechting and Flanders, 1989).

Though Blank (1978) reported that compensation of the vergence signal can be computed from knowledge of θ_H, this fact does not indicate how the biological system actually

compensates. *In vivo*, there may be many sources of compensation, e.g., accomodation cues. However, in this section we restrict our treatment to compensation that uses the cyclopean retinotopic angular variable θ_H and the extraretinal eye position vergence signal γ. The observation that compensation is poorer at greater distances suggests that the compensation could depend on both θ_H and γ, because the sensitivity of the latter variable becomes lower at larger distances (Figure 2a). Thus we propose that an egocentric distance estimate invariant under changes of the retinotopic angle θ_H is computed by combining extraretinal information about vergence with information about θ_H. Moreover, head movements made during VOR fixation are used to generate the many combinations of θ_H and γ associated with a target of fixed distance from the body. In short, we show that a network structurally analogous to the Figure 7 network, and similarly coordinated with the VOR fixation system, can readily learn to transform a θ_H-dependent estimate of target distance (namely vergence) into an invariant body-centered estimate of true target distance R_B. Because the network learns a nonlinear mapping, it also illustrates how nature may use supplementary networks to correct residual errors, resulting from nonlinearities, in the representations of horizontal and vertical angles learned by the faster linear mapping networks of the previous section.

Unlike Figure 7 where agonist-antagonist representations of neck muscle commands sample errors at the DV stage, in Figure 12 a topographic map representing θ_H and γ samples errors at the DV stage. The following paragraphs describe model components mathematically.

Figure 12

The antagonistic pair of activities h_5 and h_6 form a head-centered representation of target distance from the head. These activities are defined according to the equations:

$$h_5 = r_1 - l_1 \tag{19}$$

$$h_6 = \gamma_{\max} - h_5 \tag{35}$$

where $\gamma_{\max}$ is the largest value of h_5 encountered in the workspace, and r_1 and l_1 are the normalized eye muscle length activities described in Section 3. Activity h_5 is thus directly related to vergence.

In the (θ_H, γ) topographic map, each cell codes a small range of (θ_H, γ) values, as represented by the antagonistic pairs (h_1, h_2) and (h_5, h_6). That is, a cell in the map fires with activity t_i at its maximal level (i. e., $t_i = 1$) if the values of both θ_H and γ are within small ranges specific to that cell. The cell fires with less activity for nearby values of θ_H and γ, and the cell does not fire at all if θ_H and γ are well outside this small range. Examples of networks capable of forming topographic maps from agonist-antagonist pairs such as

(h_1, h_2) and (h_5, h_6) are described in Kohonen (1984, Chapter 5) and Grossberg and Kuperstein (1986, 1989, Chapter 6). The (θ_H, γ) map used in the simulations contained 750 cells, corresponding to 50 regions of θ_H and 15 regions of γ. Five map cells were active for each input (one maximally and the others to lesser degrees), and the total activity of the active map cells was 2.0.

The remainder of the activity equations were essentially the same as in Section 5. For completeness, these equations are included below, with index $i = 5$ or 6.

DV Activity

$$x_i = h_i + \sum_{j=1}^{N} t_j z_{ji} - b_i^{(1)}, \tag{36}$$

where N is the number of cells in the (γ, θ_H) map.

Body-Centered Activity

$$b_i^{(1)} = h_i + \sum_{j=1}^{N} t_j z_{ji}. \tag{37}$$

Gated Updating of Body-Centered Activity

$$\frac{d}{dt} b_i^{(1)} = G([x_i]^+ - [x_j]^+). \tag{38}$$

Normalized Body-Centered Activity

$$b_5^{(2)} = \frac{b_5^{(1)}}{b_5^{(1)} + b_6^{(1)}} \quad \text{and} \quad b_6^{(2)} = \frac{b_6^{(1)}}{b_5^{(1)} + b_6^{(1)}}. \tag{39}$$

The simulations used the

Learning Law

$$\frac{d}{dt} z_{ji} = -\epsilon_2 t_j [-F z_{ji} + x_i], \tag{40}$$

where $i \epsilon \{5, 6\}$ and $j = 1, 2, \ldots, N$.

The training procedure used in this section is essentially as described in Section 4. Specifically,

1) Initialize all weights to 0.0.

2) Choose a random initial head position (θ_N, ϕ_N).

3) Choose a random target position (θ_T, ϕ_T, R_T).

4) Foveate new target by adjusting h_i so that $\theta_H = \theta_T - \theta_N$ and $\phi_H = \phi_T - \phi_N$. Upon fixation of the new target, transiently activate signal G and update the body coordinate populations $b_i^{(1)}$ and $b_i^{(2)}$, $i = 1, 2, \ldots, 6$.

5) Choose a new head position while remaining foveated on current target by changing n_{ij} and adjust h_i accordingly to keep $\theta_H + \theta_N = \theta_T$ and $\phi_H + \phi_N = \phi_T$. This step corresponds to moving the head while using the VOR to keep the target foveated. The new head position is chosen from a uniform random distribution centered at $\theta_N = 0$.

6) Adjust weights from the (θ_H, γ) map populations to the head-neck DV populations according to equation (42). Learning occurs when the head position remains fixed at the end of the movement. (Learning could also occur during the movement, as in Section 7.)

7) Repeat steps (3)–(7) until the learning process converges.

Again, a fourth-order Runge-Kutta method of integration was used, with $\Delta t = 0.01$ and a total integration time of 0.1 per trial. Learning parameters $F = 0.01$ and $\epsilon_2 = 2.0$ were chosen.

Figure 13

Figure 13 shows the average error in inches of the internal representation of R_B throughout the workspace ($-40° < \theta_H < 40°$, 10 in. $< R <$ 30 in.). Error was found by sweeping over a range of θ_H values for a fixed $b_i^{(2)}$ value, searching for the distance R_B which corresponded to this $b_i^{(2)}$ value at each θ_H value, computing the difference between this distance and the distance found for $\theta_H = 0$, and averaging the absolute values of such differences over many values of $b_i^{(2)}$ and θ_H. The average error for the body-centered representation of R falls below 0.2 inches after 10,000 trials. Figure 14 shows the egocentric distances R_B that result in constant $b_5^{(2)}$ and $b_6^{(2)}$ values for targets at head-centered horizontal angle θ_H between $-40°$ and $+40°$ after 20,000 learning trials. Values are plotted for $b_i^{(2)}$ corresponding to R_B = 10, 15, 20, 25, and 30 inches. Unlike Figure 11, which shows different values of R_B corresponding to the same vergence and therefore to the same head-centered representation of distance, Figure 14 shows that the same target distance corresponds to a fixed body-centered representation of distance independent of head angle. By simply looking at many fixed targets while moving the head, the network has learned to invariantly represent distance from the body despite changes in head position.

Figure 14

9. Concluding Remarks

An invariant body-centered representation of target positions in 3-D space can be used to plan limb and coordinated eye-head movements to a spatial target without regard for the position of the eyes in the head or the head on the torso while visually perceiving the target. A head-centered cyclopean representation of foveated target position that incorporates

vergence and spherical coordinate angles arises naturally from sums and differences of oculomotor signals and also correlates well with the geometry of the vestibular system. Greve, Grossberg, Guenther, and Bullock (1993) discussed psychophysical data supporting the existence of such a vergence-spherical coordinate frame, particularly data concerning the role of an extraretinal vergence signal (Blank, 1978; Foley, 1980). Consistent neurophysiological data include the head-centered vector representation in the caudal midbrain and medulla of the frog (Grobstein, 1991). By using a distance signal based on vergence, the representation devotes the majority of its dynamic range to nearby targets. This efficiently uses limited neural circuitry by accurately representing target positions within an observer's reach while more roughly approximating positions that are further away. Grossberg, Guenther, Bullock, and Greve (1992) showed how this spatial representation could include non-foveated targets by learning to combine retinal and extraretinal motor information invariantly under movements of the eyes. The present article has addressed the problem of transforming this head-centered representation into a body-centered representation that is invariant under movements of the head.

The anatomy of the spinal column, which favors head movements around preferred axes, also suggests the usefulness of an egocentric coordinate frame based on cyclopean spherical coordinate angles. Head movements along these preferred axes are almost linearly related to the internal compensations needed to transform head-centered representations into invariant body-centered representations. Fast learning of such a transformation was demonstrated herein using a self-organizing neural network. By simply foveating and changing head position for approximately 200 targets, the network learns an invariant representation of horizontal and vertical angles of the target with respect to a body-centered spherical coordinate frame. Although target distance from the head is approximately equal in the head-centered and body-centered spherical coordinate frames, a residual nonlinear error exists in this transformation for a representation of target distance based on vergence. An augmented network was described, operating according to the same principles, that is capable of autonomously learning a nonlinear correction for this error. This network operates on a slower time frame, requiring approximately 10,000 targets to build the invariant representation. A similar nonlinear learning mechanism could be used to compensate for any residual errors due to nonlinearities not handled by the faster linear mapping network in transforming from head-centered to body-centered horizontal and vertical angles.

Because the spherical coordinate frames described here correspond closely to spatial representation by the vestibular system, they should be well suited to relating head-centered or body-centered coordinates to a world-based coordinate frame. Recent models of hippocam-

pal function for navigation (McNaughton, Chen, and Marcus, 1991; O'Keefe, 1990) utilize a polar egocentric reference frame whose coordinates correspond to the coordinates θ_{II} and R_{II} in the representation described herein. Furthermore, data from Taube, Muller, and Ranck (1990a, 1990b) identify head-direction cells in rat postsubiculum that code world-centered head direction, which provides the type of information needed to transform egocentric angle θ_{II} into a world-based framework.

REFERENCES

Alexander, G.E. and Crutcher, M.D. (1990a). Neural representations of the target (goal) of visually guided arm movements in three motor areas of the monkey. *Journal of Neurophysiology*, **64**(1), 164–178.

Alexander, G.E. and Crutcher, M.D. (1990b). Preparation for movement: Neural representations of intended direction in three motor areas of the monkey. *Journal of Neurophysiology*, **64**(1), 133–150.

Bernstein, N.A. (1967). **The co-ordination and regulation of movements**. New York: Pergamon Press.

Bizzi, E., Kalil, R.E., and Tagliasco, V. (1971). Eye-head coordination in monkeys: Evidence for centrally patterned organization. *Science*, **173**, 452–454.

Blank, A.A. (1978). Metric geometry in human binocular perception: Theory and fact. In E.L.J. Leeuwenberg and H.F.J.M. Buffart (Eds.), **Formal theories of visual perception**. New York: Wiley and Sons.

Blanks, R.H.I., Curthoys, I.S., Bennett, M.L., and Markham, C.H. (1985). Planar relationships of the semicircular canals in rhesus and squirrel monkeys. *Brain Research*, **340**, 315–324.

Bullock, D. and Grossberg, S. (1988). Neural dynamics of planned arm movements: Emergent invariants and speed-accuracy properties during trajectory formation. *Psychological Review*, **95**(1), 49–90.

Bullock, D., Grossberg, S., and Guenther, F.H. (1993). A self-organizing neural model of motor equivalent reaching and tool use by a multijoint arm. *Journal of Cognitive Neuroscience*, **5**, 408–435.

Caminiti, R., Johnson, P., and Urbano, A. (1990). Making arm movements within different parts of space: Dynamic aspects in the primate motor cortex. *Journal of Neuroscience*, **10**, 2039–2058.

Carpenter, G.A. and Grossberg, S. (1987). A massively parallel architecture for a self-organizing neural pattern recognition machine. *Computer Vision, Graphics, and Image Processing*, **37**, 54–115.

Carpenter, G.A. and Grossberg, S. (Eds.) (1991). **Pattern recognition by self-organizing neural networks**. Cambridge, MA: MIT Press.

Crutcher, M.D. and Alexander, G.E. (1990). Movement-related neuronal activity selectively coding either direction or muscle pattern in three motor areas of the monkey. *Journal of Neurophysiology*, **64**(1), 151–163.

DeValois, R.L. and DeValois, K.K. (1975). Neural coding of color. In E. C. Carterette and M. P. Friedman (Eds.), **Handbook of perception, Volume 5: Seeing**. New York: Academic Press.

Dichgans, J., Bizzi, E., Morasso, P., and Tagliasco, V. (1973). Mechanisms underlying recovery of eye-head coordination following bilateral labyrinthectomy in monkeys. *Experimental Brain Research*, **18**, 548–562.

Ezure, K. and Graf, W. (1984). A quantitative analysis of the spatial organization of the vestibulo-ocular reflexes in lateral- and frontal-eyed animals, I: Orientation of semicircular canals and extraocular muscles. *Neuroscience*, **12**, 85–93.

Foley, J.M. (1980). Binocular distance perception. *Psychological Review*, **87**, 411–434.

Gaudiano, P. and Grossberg, S. (1991). Vector associative maps: Unsupervised real-time error-based learning and control of movement trajectories. *Neural Networks*, **4**, 147–183.

Georgopoulos, A.P., Kalaska, J.F., Caminiti, R., and Massey, J.T. (1982). On the relations between the direction of two-dimensional arm movements and cell discharge in primate motor cortex. *Journal of Neuroscience*, **2**, 1527–1537.

Georgopoulos, A.P., Kalaska, J.F., Crutcher, M.D., Caminiti, R., and Massey, J.T. (1984). The representation of movement direction in the motor cortex: Single cell and population studies. In G.M. Edelman, W.E. Gall, and W.M. Cowan (Eds.), **Dynamic aspects of neocortical function**. New York: Wiley and Sons, pp. 501–524.

Goodale, M.A. and Milner, D. (1992). Separate visual pathways for perception and action. *Trends in Neurosciences*, **15**, 20–25.

Graf, W. (1988). Motion detection on physical space and its peripheral and central representation. In B. Cohen and V. Henn (Eds.), **Representation of three-dimensional space in the vestibular, oculomotor, and visual systems**. New York: New York Academy of Sciences, **545**, pp. 154–169.

Greve, D., Grossberg, S., Guenther, F.H., and Bullock, D. (1993). Neural representations for sensory-motor control, I: Head-centered 3-D target positions from opponent eye commands. *Acta Psychologica*, **82**, 115–138.

Grobstein, P. (1991). Directed movement in the frog: A closer look at a central representation of spatial location. In M.A. Arbib and J.-P. Ewert (Eds.), **Visual structure and integrated functions**. Berlin: Springer-Verlag, pp. 125–138.

Grobstein, P. and Staradub, V. (1989). Frog orienting behavior: The descending distance signal. *Society for Neuroscience Abstracts*, **15**, 54.

Grossberg, S. (1969). Embedding fields: A theory of learning with physiological implications.

Journal of Mathematical Psychology, **6**, 209–239.

Grossberg, S. (1976a). Adaptive pattern classification and universal recoding, I: Parallel development and coding of neural feature detectors. *Biological Cybernetics*, **23**, 121–134.

Grossberg, S. (1976b). Adaptive pattern classification and universal recoding, II: Feedback, expectation, olfaction, and illusions. *Biological Cybernetics*, **23**, 187–202.

Grossberg, S. (1982). **Studies of mind and brain: Neural principles of learning, perception, development, cognition, and motor control.** Boston: Reidel Press.

Grossberg, S., Guenther, F.H., Bullock, D., and Greve, D. (1993). Neural representations for sensory-motor control, II: Learning a head-centered visuomotor representation of 3-D target positions. *Neural Networks*, **6**, 43–67.

Grossberg, S. and Kuperstein, M. (1986). **Neural dynamics of adaptive sensory-motor control: Ballistic eye movements.** Amsterdam: Elsevier/North-Holland.

Grossberg, S. and Kuperstein, M. (1989). **Neural dynamics of adaptive sensory-motor control: Expanded edition.** Elmsford, NY: Pergamon Press.

Hebb, D.O. (1949). **The organization of behavior.** New York: Wiley and Sons, pp. 153–157.

Hodgkin, A.L. (1964). **The conduction of the nervous impulse.** Liverpool: Liverpool University Press.

Hollerbach, J.M., Moore, S.P., and Atkeson, C.G. (1986). Workspace effect in arm movement kinematics derived by joint interpolation. In G. Gantchev, B. Dimitrov, and P. Gatev (Eds.). **Motor control.** New York: Plenum Press.

Kalaska, J.F. and Crammond, D.J. (1992). Cerebral cortical mechanisms of reaching movements. *Science*, **255**, 1517–1523.

Kandel, E.R. (1985). Processing of form and movement in the visual system. In E.R. Kandel and J.H. Schwartz (Eds.), **Principles of neural science.** New York: Elsevier, pp. 366–383.

Katz, B. (1966). **Nerve, muscle, and synapse.** New York: McGraw-Hill.

Kohonen, T. (1984). Self-organization and associative memory. New York, NY: Springer-Verlag.

Levy, W. and Desmond, N. (1985). The rules of elemental synaptic plasticity. In W. Levy, J. Anderson, and S. Lehmkuhle (Eds.), **Synaptic modification, neuron selectivity, and nervous system organization.** Hillsdale, NJ: Erlbaum Associates, pp. 105–122.

Masino, T. and Grobstein, P. (1989). The organization of descending tectofugal pathways underlying orienting in the frog, *Rana pipiens*, I: Lateralization, parcellation, and an inter-

mediate spatial representation. *Experimental Brain Research*, **75**, 227–244.

Masino, T. and Knudsen, E.I. (1990). Horizontal and vertical components of head movement are controlled by distinct neural circuits in the barn owl. *Nature*, **345**, 434–437.

Mays, L.E. and Sparks, D.L. (1980). Saccades are spatially, not retinocentrically, coded. *Science*, **208**, 1163–1165.

McNaughton, B.L., Chen, L.L., and Markus, E.J. (1991). "Dead reckoning", landmark learning, and the sense of direction: A neurophysiological and computational hypothesis. *Journal of Cognitive Neuroscience*, **3**, 190–202.

Mishkin, M., Ungerleider, L.G., and Macko, K.A. (1983). Object vision and spatial vision: Two cortical pathways. *Trends in Neurosciences*, **6**, 414–417.

Mollon, J.D. and Sharpe, L.T. (1983). **Colour vision**. New York: Academic Press.

Morasso, P., Bizzi, E., and Dichgans, J. (1973). Adjustment of saccade characteristics during head movements. *Experimental Brain Research*, **16**, 492–500.

O'Keefe, J. (1990). A computational theory of the hippocampal cognitive map. *Progress in Brain Research*, **83**, 301–312.

Rauschecker, J.P. and Singer, W. (1979). Changes in the circuitry of the kitten's visual cortex are gated by postsynaptic activity. *Nature*, **280**, 58–60.

Rojer, A.S. and Schwartz, E.L. (1990). Design considerations for a space-variant visual sensor with complex-logarithmic geometry. In **10th international conference on pattern recognition, Volume 2**, pp. 278–285.

Sakata, H., Shibutani, H., and Kawano, K. (1980). Spatial properties of visual fixation neurons in posterior parietal association cortex of the monkey. *Journal of Neurophysiology*, **43**, 1654–1672.

Singer, W. (1983). Neuronal activity as a shaping factor in the self-organization of neuron assemblies. In E. Basar, H. Flohr, H. Haken, and A.J. Mandell (Eds.), **Synergetics of the brain**. New York: Springer-Verlag, pp. 89–101.

Soechting, J. F. and Flanders, M. (1989). Errors in pointing are due to approximations in sensorimotor transformation. *Journal of Neurophysiology*, **62**, 595–608.

Taub, J.S., Muller, R.U., and Ranck, J.B.J. (1990a). Head-direction cells recorded from the postsubiculum in freely moving rats, I: Description and quantitative analysis. *Journal of Neuroscience*, **10**, 420–435.

Taub, J.S., Muller, R.U., and Ranck, J.B.J. (1990b). Head-direction cells recorded from the postsubiculum in freely moving rats, II: Effects of environmental manipulations. *Journal of*

Neuroscience, **10**, 436–447.

Tomlinson, R.D. and Bahra, P.S. (1986). Combined eye-head gaze shifts in the primate, II: Interactions between saccades and the vestibulo-ocular reflex. *Journal of Neurophysiology*, **56**, 1558–1570.

Ungerleider, L.G. and Mishkin, M. (1982). Two cortical visual systems: Separation of appearance and location of objects. In D.L. Ingle, M.A. Goodale, and R.J.W. Mansfield (Eds.), **Analysis of visual behavior**. Cambridge, MA: MIT Press, pp. 549–586.

Vidal, P.P., de Waele, C., Graf, W., and Berthoz, A. (1988). Skeletal geometry underlying head movements. In B. Cohen and V. Henn (Eds.), **Representation of three-dimensional space in the vestibular, oculomotor, and visual systems**. New York: New York Academy of Sciences, **545**, pp. 228–238.

Vidal, P.P., Graf, W., and Berthoz, A. (1986). The orientation of the cervical vertebrate column in unrestrained awake animals, I: Resting position. *Experimental Brain Research*, **61**, 549–559.

FIGURE CAPTIONS

Figure 1. The geometry of 3-D target of localization by the two eyes: Symbols L and R are the centers of the left and right eyes. Left side shows how a closer target generates a larger vergence angle. Right side shows how the vergence angle is calculated from the angles of the eyes in their orbits.

Figure 2. (a) Vergence as a function of target radius for a target on the line passing through the midpoint between the eyes (the cranial egocenter) and projecting straight ahead. (b) Distance-response curves for a class of visual fixation neurons in posterior parietal cortex (area 7a, posterior part). Reprinted with permission from Sakata *et al.* (1980). (c) Visual acuity as a function of angular distance from the fovea (adapted from Kandel, 1985). The similar shapes of the curves in (a) and (c) suggest that the nervous system may use a similar strategy to efficiently represent retinotopic and body-centered space with limited neural circuitry.

Figure 3. Spherical coordinate frame for specifying a target position with respect to the head. This coordinate frame is related to the head-centered representation of space described in Section 3.

Figure 4. Geometry of cyclopean position: The angles θ_L and θ_R that the left eye and right eye assume to foveate a target correspond to a cyclopean, head-centered angle θ_H.

Figure 5. Opponent processing architecture for the calculation of the internal representation of gaze angle (h_2) and vergence (h_5). Signals L_1, L_2, R_1, and R_2 are corollary discharges from the outflow movement cells that control eye position. The muscles are arranged in agonist-antagonist pairs. Stimulation by neuron L_2 causes a contraction of the left medial muscle, which rotates the left eyeball to the right. The activity of each pair of cells is normalized at cells l_1, l_2, r_1, and r_2.

Figure 6. Top view (a, b, c) and side view (d, e, f) showing relationships between the head-centered coordinates (subscript H), body-centered coordinates (subscript B), and head angles with respect to the body (subscript N).

Figure 7. Network for learning transformation from a head-centered spherical coordinate representation to a body-centered spherical coordinate representation of target position.

Figure 8. Average error for (a) θ and (b) ϕ using excitatory pathways from the neck muscles and a uniform distribution for choosing new head position.

Figure 9. Results after 20 learning trials. The left side shows the internally represented body-centered target position as the head is moved through over 30° of both horizontal and vertical angle. The right side shows the actual target position. The change in represented target position as the head is moved indicates that the network has not yet learned to invariantly represent body-centered target position.

Figure 10. Results after 200 learning trials. The left side shows the internally represented body-centered target position as the head is moved through over 30° of both horizontal and vertical angle. The right side shows the actual target position. The internal representation is now invariant under head movements.

Figure 11. Actual positions of foveated objects which give rise to constant values of vergence (curved lines) for different head angles. Without the networks described in this section, an internal estimate of distance from the head for a fixed target based solely on vergence would suffer from the variability due to head position seen here. Human perception of distance is better than these isovergence-based estimates, particularly for nearer distances (Blank, 1978).

Figure 12. Network for learning to use spatial map of θ_H and γ values to improve a body-centered estimate of a foveated target's radial distance R_B.

Figure 13. Average error of internal estimate of R_B during learning by the network of Figure 12.

Figure 14. Actual positions of foveated objects giving rise to internal R_B estimates of 10, 15, 25, and 30 inches after learning by the network of Figure 12. The network has learned to represent distance from the head invariantly across horizontal changes in head angle.

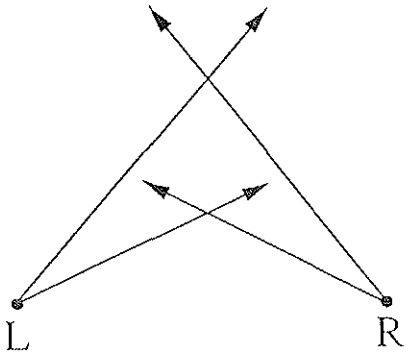

(a)

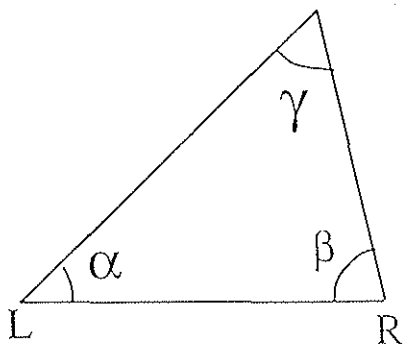

$\gamma = 180 - (\alpha + \beta)$

(b)

Figure 1

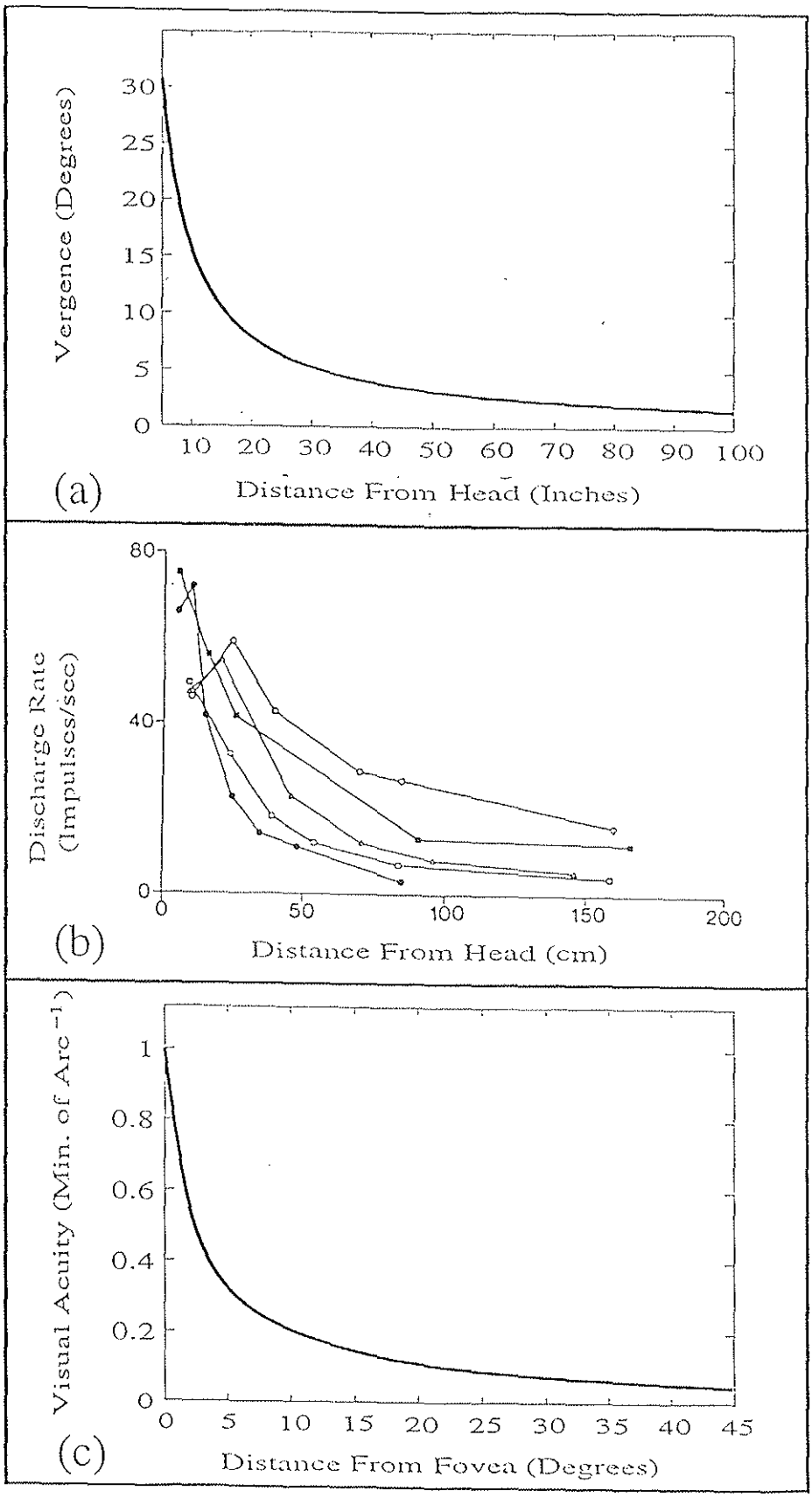
Vergence (Degrees)
30
25
20
15
10
5
0
10 20 30 40 50 60 70 80 90 100
(a)
Distance From Head (Inches)
Discharge Rate (Impulses/sec)
80
40
0
0 50 100 150 200
(b)
Distance From Head (cm)
Visual Acuity (Min. of Arc^{-1})
1
0.8
0.6
0.4
0.2
0
0 5 10 15 20 25 30 35 40 45
(c)
Distance From Fovea (Degrees)

Figure 2

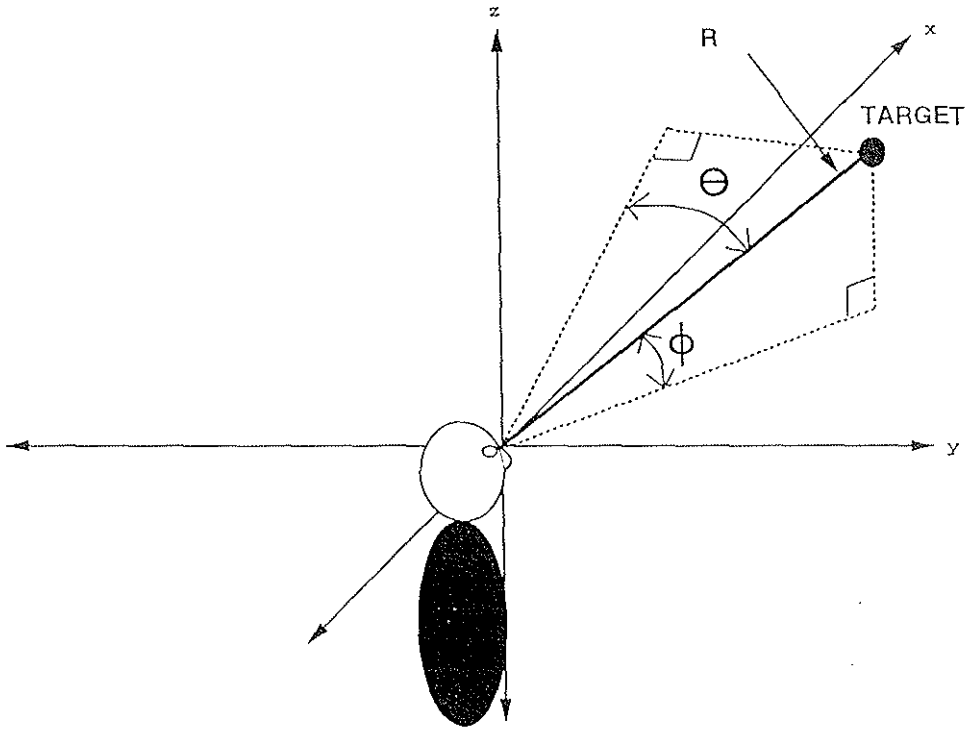

Figure 3

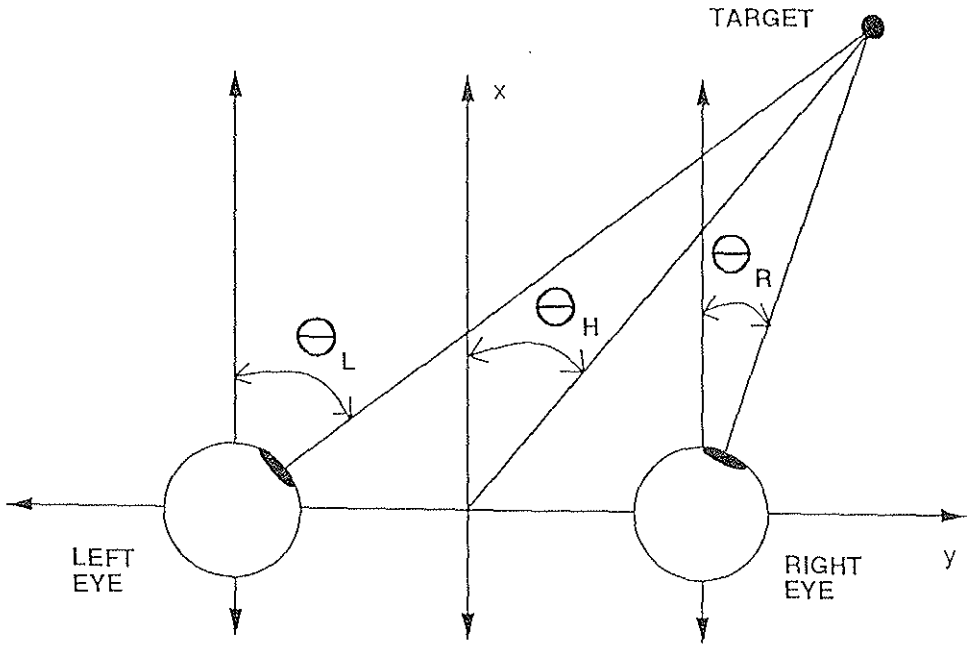

Figure 4

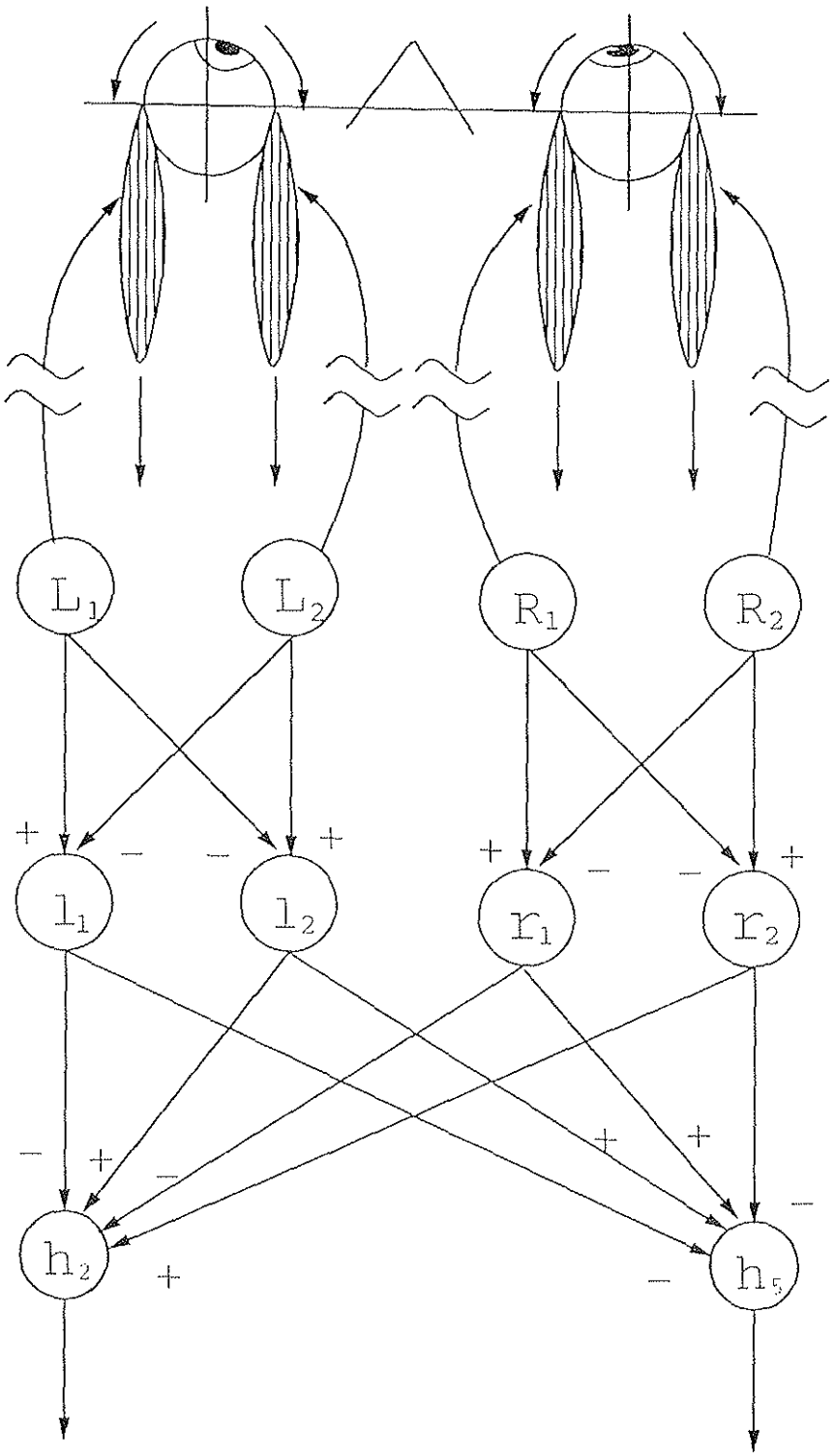

Figure 5

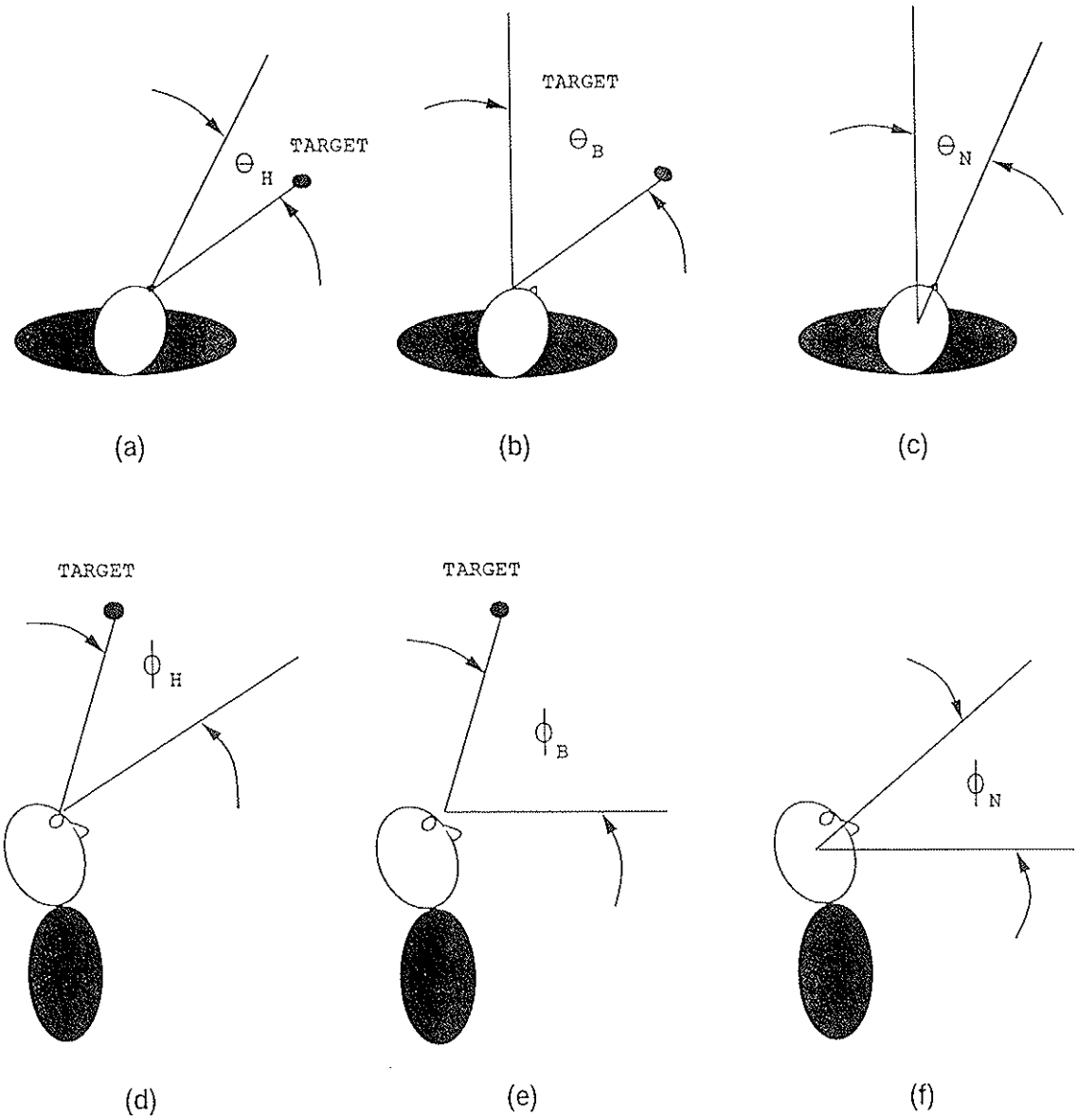
TARGET
Θ_H
TARGET
Θ_B
Θ_N
(a)
(b)
(c)
TARGET
ϕ_H
TARGET
ϕ_B
ϕ_N
(d)
(e)
(f)

Figure 6

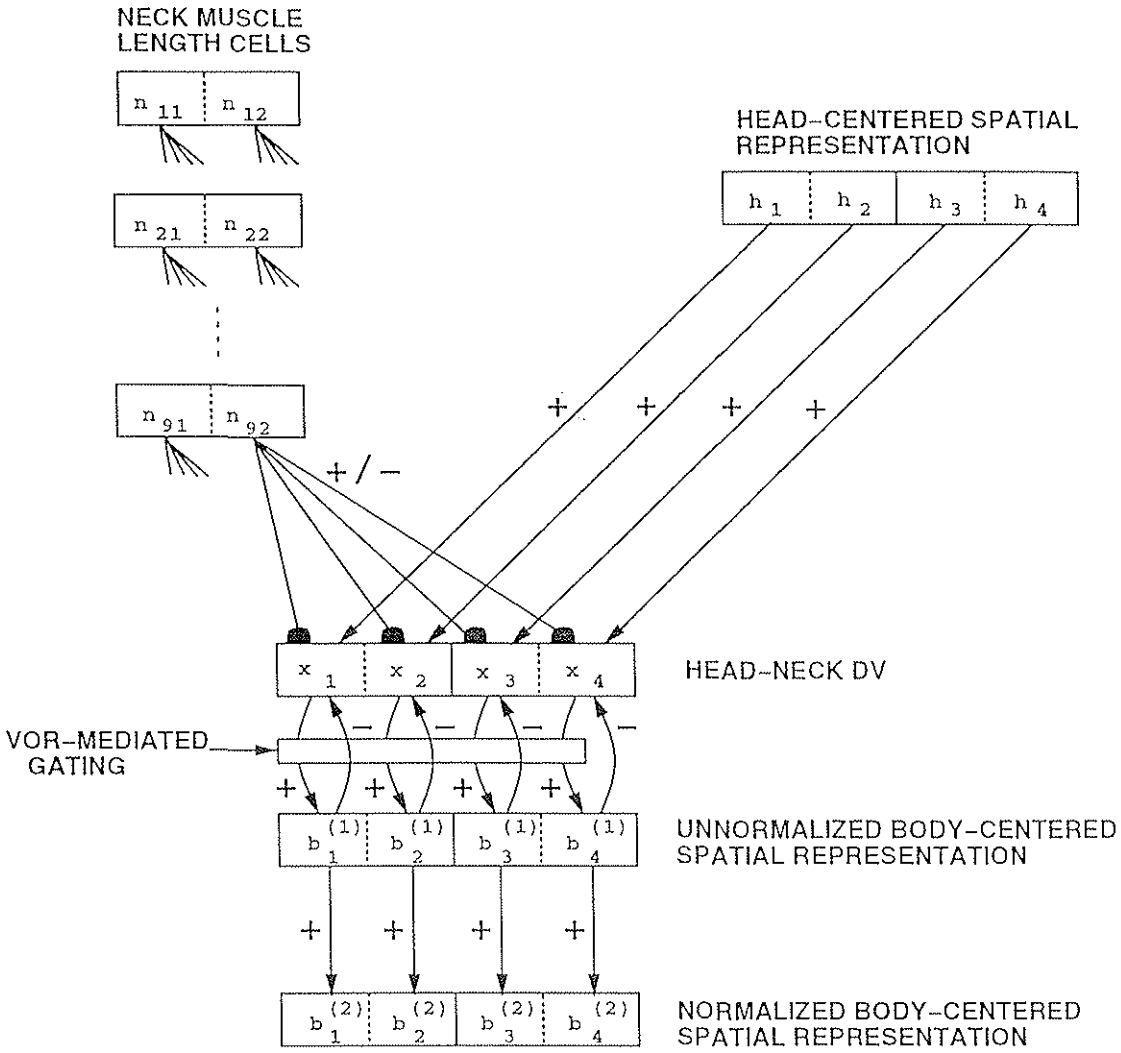
NECK MUSCLE
LENGTH CELLS
n 11
n 12
n 21
n 22
n 91
n 92
+/−
HEAD-CENTERED SPATIAL
REPRESENTATION
h 1
h 2
h 3
h 4
+
+
+
+
x 1
x 2
x 3
x 4
HEAD-NECK DV
VOR-MEDIATED
GATING
−
−
−
−
+
+
+
+
b 1 (1)
b 2 (1)
b 3 (1)
b 4 (1)
UNNORMALIZED BODY-CENTERED
SPATIAL REPRESENTATION
+
+
+
+
b 1 (2)
b 2 (2)
b 3 (2)
b 4 (2)
NORMALIZED BODY-CENTERED
SPATIAL REPRESENTATION

Figure 7

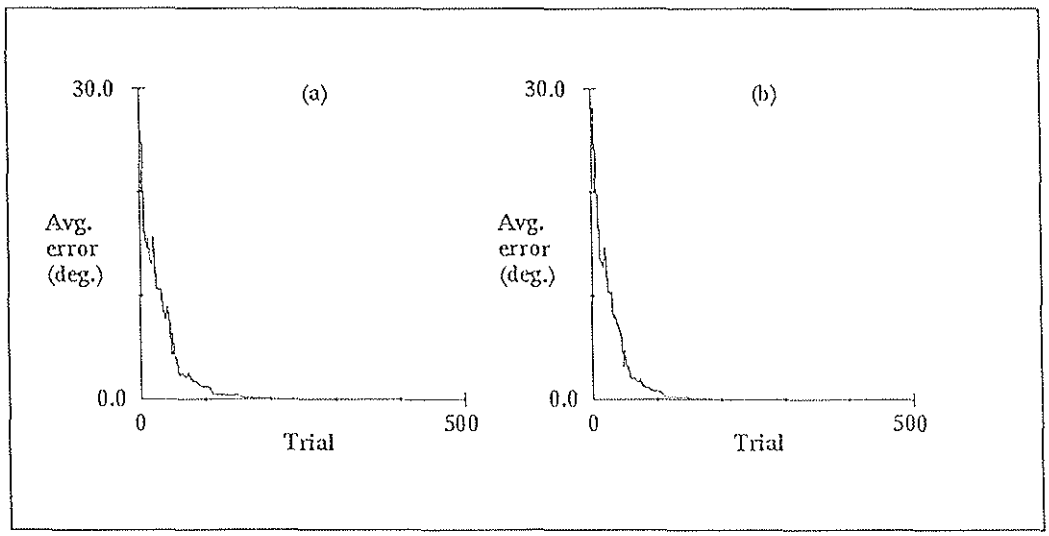
30.0
(a)
Avg.
error
(deg.)
0.0
0
500
Trial
30.0
(b)
Avg.
error
(deg.)
0.0
0
500
Trial

Figure 8

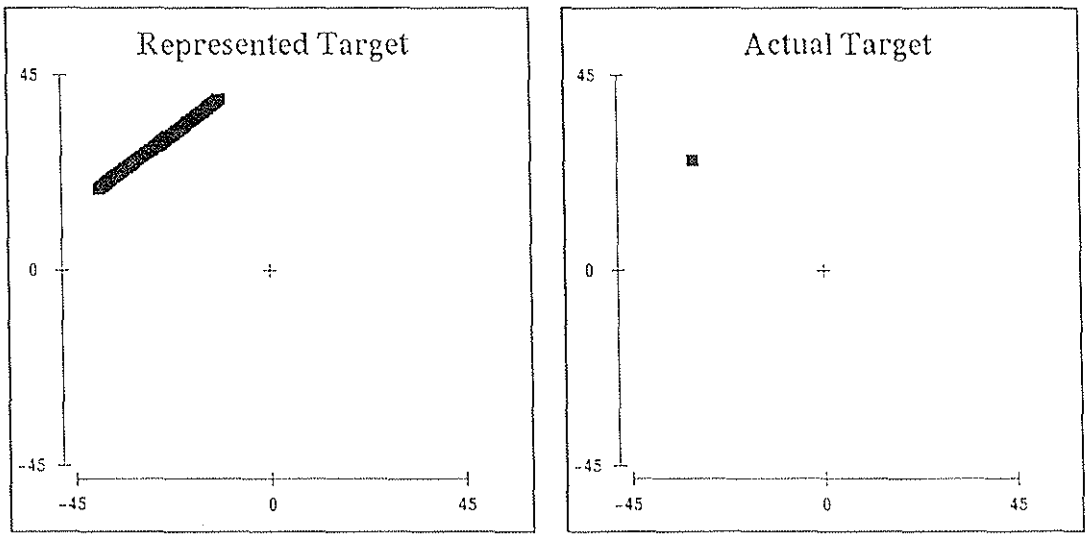

Figure 9

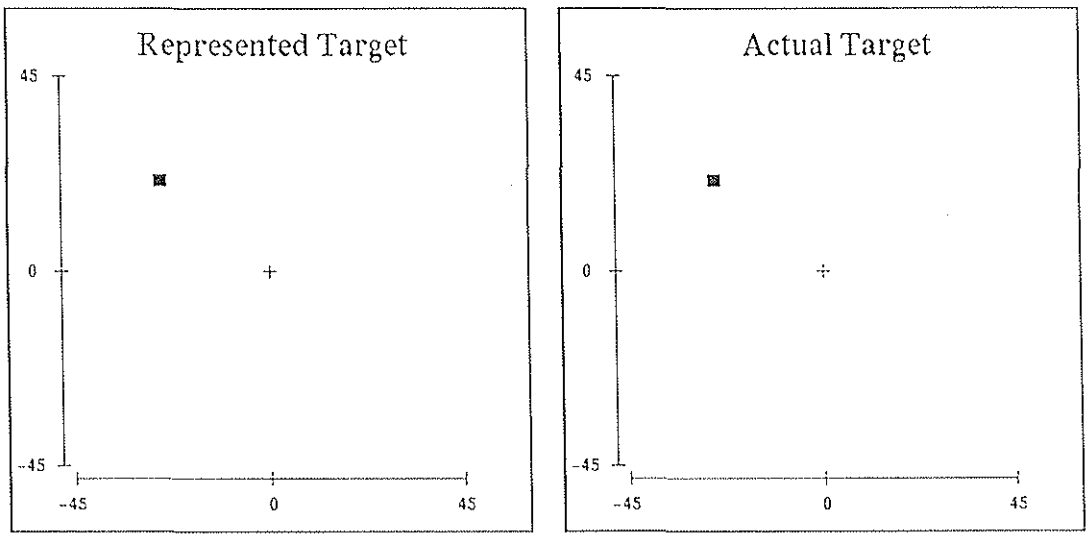

Figure 10

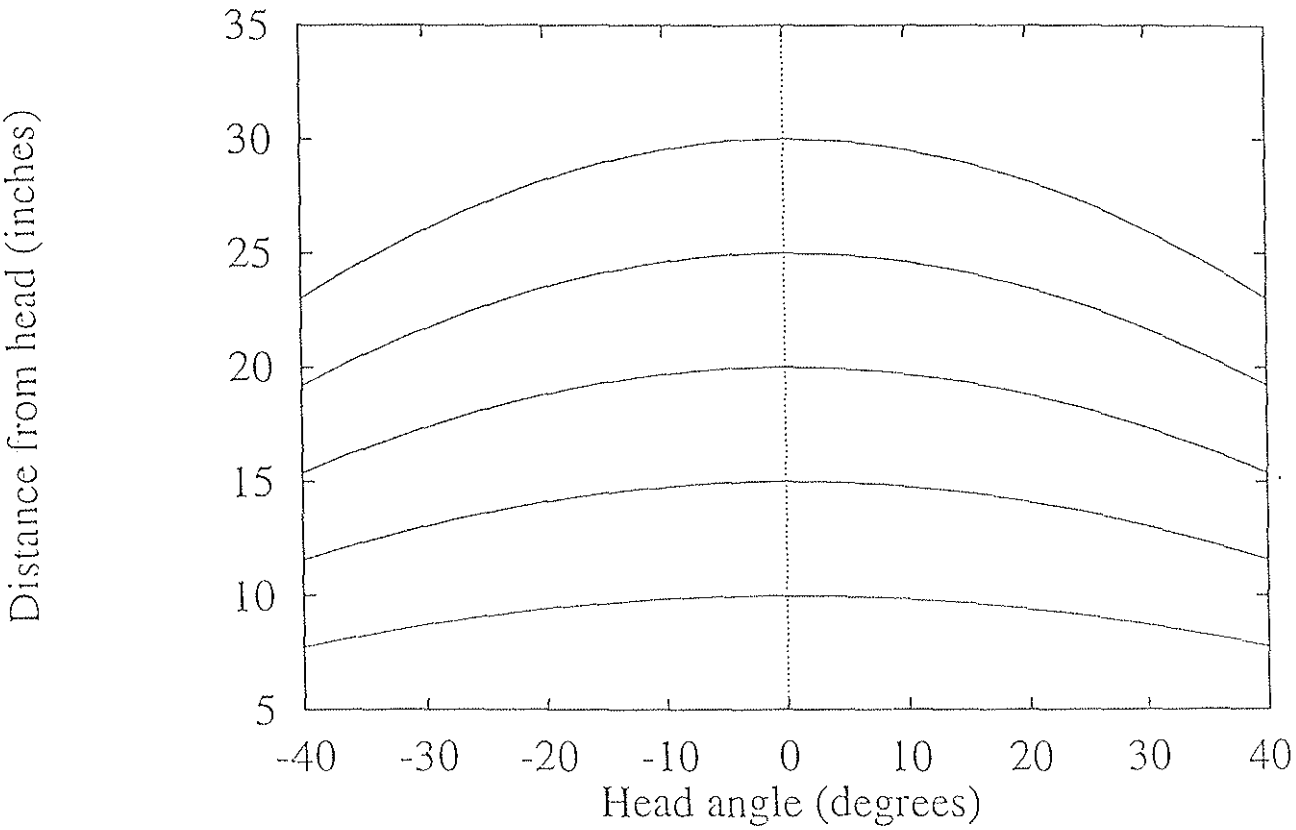
Distance from head (inches)
35
30
25
20
15
10
5
-40
-30
-20
-10
0
10
20
30
40
Head angle (degrees)

Figure 11

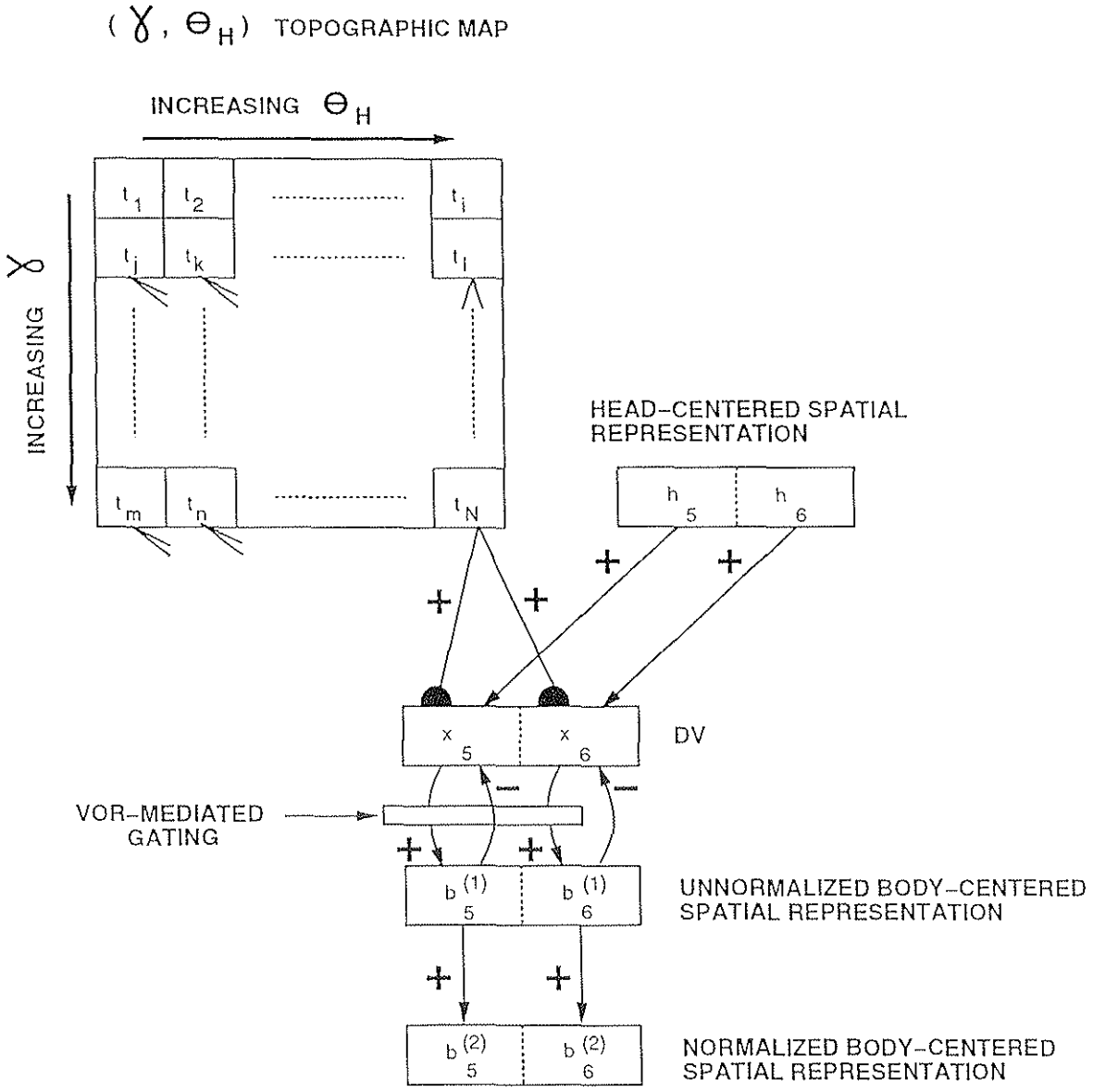
(γ , Θ H) TOPOGRAPHIC MAP
INCREASING Θ H
INCREASING γ
t 1
t 2
t i
t j
t k
t l
t m
t n
t N
HEAD-CENTERED SPATIAL REPRESENTATION
h 5
h 6
x 5
x 6
DV
VOR-MEDIATED GATING
b (1) 5
b (1) 6
UNNORMALIZED BODY-CENTERED SPATIAL REPRESENTATION
b (2) 5
b (2) 6
NORMALIZED BODY-CENTERED SPATIAL REPRESENTATION

Figure 12

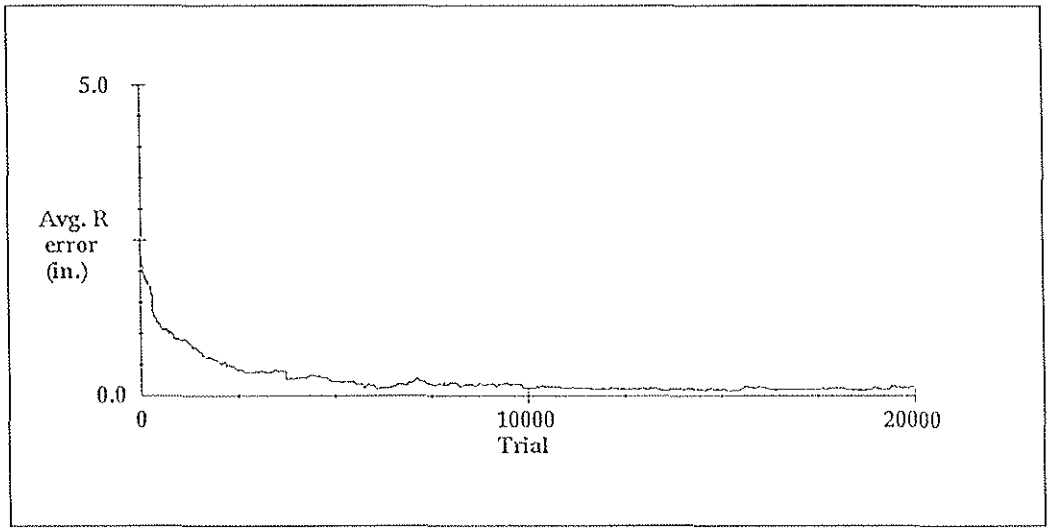

Figure 13

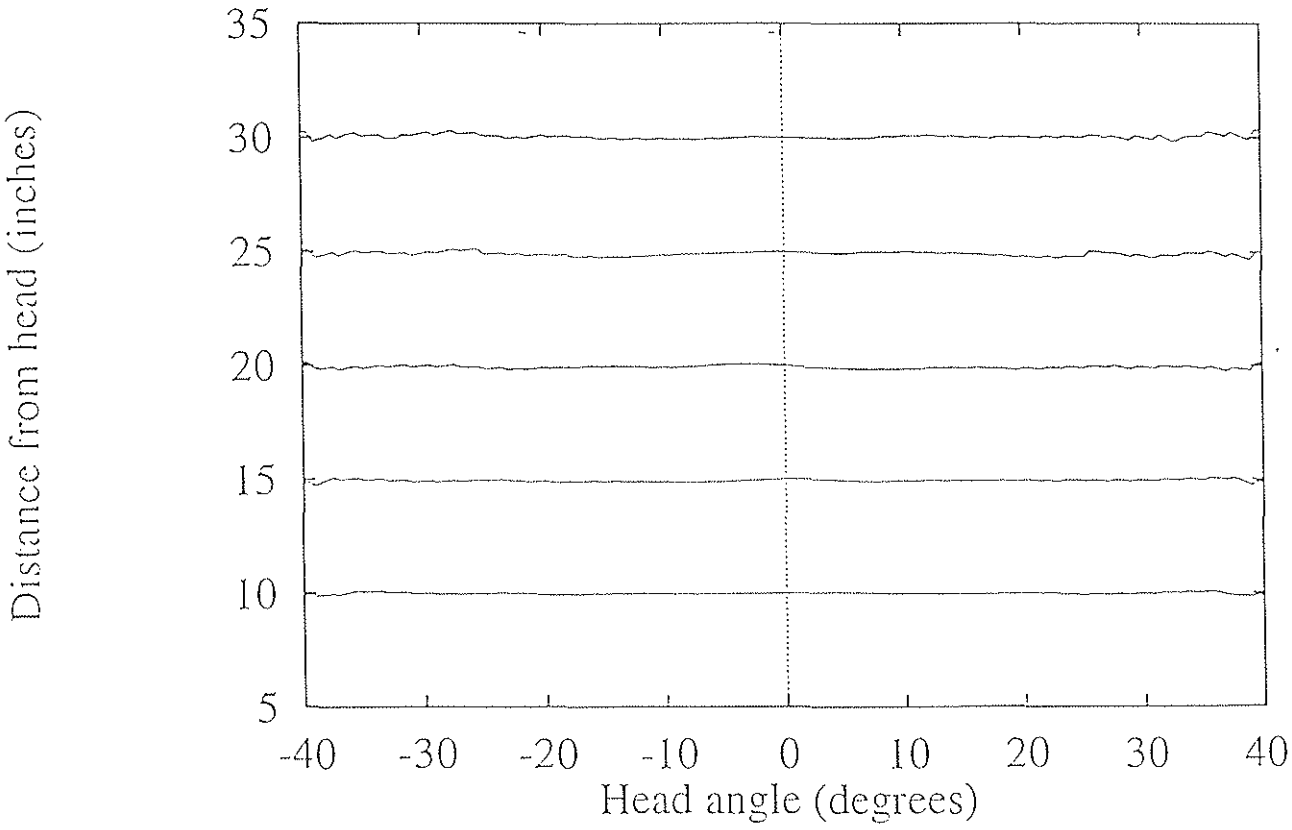
Distance from head (inches)
35
30
25
20
15
10
5
-40
-30
-20
-10
0
10
20
30
40
Head angle (degrees)

Figure 14